ELSEVIER

Spectrochimica Acta Part B 57 (2002) 1071–1099

SPECTROCHIMICA ACTA PART B

www.elsevier.com/locate/sab

Hybrid Monte Carlo—fluid modeling network for an argon/hydrogen direct current glow discharge

Annemie Bogaerts*, Renaat Gijbels

University of Antwerp, Department of Chemistry, Universiteitsplein 1, B-2610 Wilrijk-Antwerp, Belgium

Received 11 December 2001; accepted 24 May 2002

Abstract

A hybrid modeling network, consisting of several Monte Carlo and fluid models, is developed for a dc glow discharge typically used for mass spectrometry, in a mixture of Ar with 1% H_2. The species described in the model are: electrons; Ar^+ ions and fast Ar atoms; ArH^+, H^+, H_2^+ and H_3^+ ions; H atoms; and H_2 molecules; as well as Ar metastable atoms. Sixty-three reactions are taken into account in the model. The calculated densities of the various plasma species are presented. The electrons and Ar^+ ions are the dominant charged species in the plasma, with densities in the order of 10^{11} cm^{-3}. Furthermore, the ArH^+ and H_3^+ ions have a relatively high density (in the order of a few 10^{10} cm^{-3}), whereas the H^+ and H_2^+ densities are negligible (order of 10^6–10^7 cm^{-3}). The dissociation degree of the H_2 molecules was calculated to be very low (approx. 0.02%), yielding H_2 and H densities in the order of 10^{14} and 10^{11} cm^{-3}, respectively. The relative contribution of different production and loss processes of the electrons, different ions, H atoms, H_2 molecules and Ar metastable atoms are also calculated. Finally, a comparison is made between a pure Ar discharge and a glow discharge in a mixture of Ar+1% H_2.

Keywords: Glow discharge; Modeling; Ar/H_2; Monte Carlo model; Fluid model

1. Introduction

Glow discharges are used, among others, for the spectrochemical analysis of (mainly) solid materials [1,2]. Recently, there has been increasing interest in the effect of small amounts of H_2 on the analytical results of Ar glow discharges [3–8]. It has been shown that some optical emission line intensities increase while others decrease when H_2 is added [3–6]. Also, the relative sensitivity factors of different elements in glow discharge mass spectrometry (which are a measure of the ionization efficiency) appear to be influenced by the addition of H_2 [7,8]. More specifically, a better correlation could be obtained between measured relative sensitivity factors and values predicted with simple empirical equilibrium models [7,8]. This might open perspectives for the future, because accurate knowledge of relative sensitivity factors is needed for quantitative analysis [1].

*Corresponding author. Tel.: +32-3820-2377; fax: +32-3820-2376.
E-mail address: annemie.bogaerts@ua.ac.be (A. Bogaerts).

PII: S0584-8547(02)00047-2

Glow discharges and other kinds of discharge plasmas in Ar–H_2 mixtures, used for various kinds of applications, have also been investigated by other authors [9–20]. In Knewstubb and Tickner [9], Meulenbroeks et al. [10] and Mason et al. [11], the addition of H_2 was found to cause a drop in the ionization in the discharge, and in the Ar ion and electron concentrations. Different kinds of processes appear to be responsible for this drop, depending on the discharge conditions. In the expanding arc discharge plasma [10], the responsible process appears to be H-atom transfer between Ar^+ and H_2, followed by very efficient electron—ArH^+ ion recombination. In a fast flowing glow discharge, with gas mixing close to the ion exit in order not to disturb the discharge, a drop in intensity was found for all major ions, except for Cu^+, which increased in abundance [11]. In Capitelli and Dilonardo [12], it is found that the dissociation rate of H_2 was much smaller in Ar–H_2 mixtures than in pure H_2 discharges, as a result of vibration–translation energy exchanges. Moreover, it is also well recognized that the addition of H_2 affects the sputter rates in glow discharges [13,14]. The sputter yield by hydrogen ions is very low, due to their low mass. This also results in more hydrogen implantation in the metal surface [13]. On the other hand, the ArH^+ ions formed in Ar/H_2 discharges start playing an important role in sputtering, due to their higher kinetic energy than Ar^+ ions when bombarding the cathode (because they lose their energy less efficiently). For the latter reason, it was found [14] that the sputter rate reaches a maximum at 5–20% H_2 added to the Ar discharge. A number of papers have also reported the measurement of ion energy distributions in Ar/H_2 discharges [15–17]. Finally, hydrogen Balmer lines were investigated in Ar/H_2 mixtures in a Grimm-type glow discharge, to obtain information on reactions in the plasma [18], on the electron density [19] and on the electric field distribution [20].

A vast number of chemical reactions between Ar and H_2 species has also been studied for conditions typically used in discharge plasmas [21–32], providing useful information, such as cross-sections and rate coefficients, for numerical investigations of Ar/H_2 discharges. Based on these data, we have recently made a survey of all possible reactions in Ar/H_2 mixtures, to investigate qualitatively the importance of these reactions and to estimate their effect on the analytical characteristics of Ar/H_2 glow discharges [33].

There exist quite a number of papers in the literature describing the modeling of H_2 in various kinds of discharge plasmas in pure H_2 (e.g. microwave discharges, surface wave discharges, electron beam produced plasmas, glow discharges) [34–41]. In most cases, particle balance equations are used for the H, H_2*, H^-, H^+, H_2^+ and H_3^+ species (or some of these species), although Monte Carlo models are also applied, e.g. in Dexter et al. [39] and Simko et al. [40]. Discharges in a mixture of SiH_4 with H_2 have been investigated with a Particle-in-cell Monte Carlo (PIC/MC) model in Yan and Goedheer [42,43]. For Ar–H_2 plasmas, however, the number of models available in the literature appears to be rather limited. Only one model was found, and this was based on particle balance equations [44]. This model applies to a thermal Ar–H_2 plasma, which operates at discharge conditions completely different from a glow discharge.

In our paper, we present a comprehensive modeling network for an Ar–H_2 glow discharge, based on fluid models (with particle balance equations) and on Monte Carlo models for the electrons, and for the ionic species and fast Ar atoms in the cathode dark space (CDS), in order to understand the effects of H_2 on Ar glow discharges.

The glow discharge plasma under study operates under direct current (dc) conditions. The calculations are performed for the standard cell to analyze flat samples in a commercial VG9000 glow discharge mass spectrometer. The cell has a length of 1.05 cm and a diameter of 2.5 cm (see below). The discharge conditions investigated are a voltage of 1000 V, a gas pressure and temperature of 0.56 torr and 330 K. The corresponding electrical current is calculated in the order of 2 mA (see below). This value correlates well with measured values for these operating conditions. The gas mixture is Ar + 1% H_2, and is assumed constant and uniformly distributed in the discharge cell. The H_2 present in the plasma is initially all in molecular form. This can, however, change after the calculations have reached steady state. The cathode of the glow discharge cell is made of copper. Atoms and ions of the cathode material are also present in the plasma, as a result of cathode sputtering (and subsequent ionization); see below.

2. Description of the model

Ten different species are taken into account in the model including: the electrons; Ar^+, ArH^+, H^+, H_2^+ and H_3^+ ions; fast Ar atoms; H atoms; and H_2 molecules; as well as metastable Ar atoms. The behavior of these species is described with a number of Monte Carlo and fluid models. The models are coupled to each other due to the interaction processes between the species. In the following, these models will be explained in some detail, emphasizing the reactions treated in the models, and the cross-sections used for these processes. At the end of this section, the interaction between the different models will be outlined.

2.1. Monte Carlo models for the Ar^+, ArH^+, H^+, H_2^+ and H_3^+ ions and the fast Ar atoms

All the ions considered in the modeling network (Ar^+, ArH^+, H^+, H_2^+ and H_3^+) as well as the fast Ar atoms, are described with a Monte Carlo model in the CDS, on their way toward the cathode. Note that the subdivision between CDS and negative glow (NG) is made on the basis of the electric field values calculated in the electron ion fluid model (see below). More specifically, the region where the magnitude of the electric field is higher than 10 V/cm is defined here as the CDS, whereas the region where the magnitude of the electric field drops below 10 V/cm is called the NG. At the present conditions, the CDS extends until approximately 0.3–0.4 cm from the cathode, whereas the NG fills the rest of the discharge. In the CDS, the potential drops rapidly from −1000 V at the cathode to roughly zero at the end of the CDS (hence, giving rise to a strong electric field), whereas the NG is characterized by a small positive and nearly constant potential, yielding a weak electric field.

The flux of the ions entering the CDS from the NG is obtained from the fluid model (see below). The ions are then accelerated toward the cathode by the strong electric field, and they are also subject to collisions. The reactions taken into account in these Monte Carlo models are briefly mentioned here, as well as the references where the cross-sections were taken from. These cross-sections as a function of ion or atom energy are presented in Figs. 1–6. The numbers in these

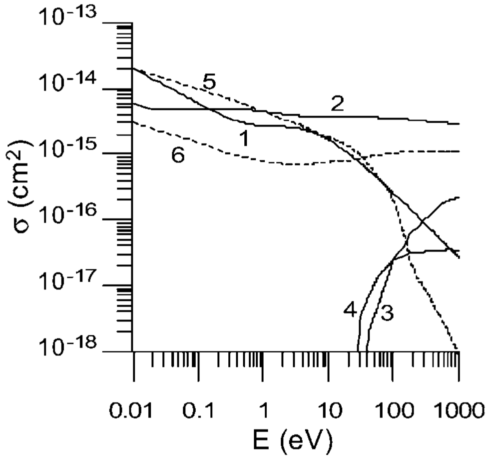

Fig. 1. Cross-sections of the Ar^+ reactions with Ar atoms (solid lines) and H_2 molecules (dashed lines) taken into account in the Ar^+ Monte Carlo model. The numbers of the curves correspond to the numbers in the text.

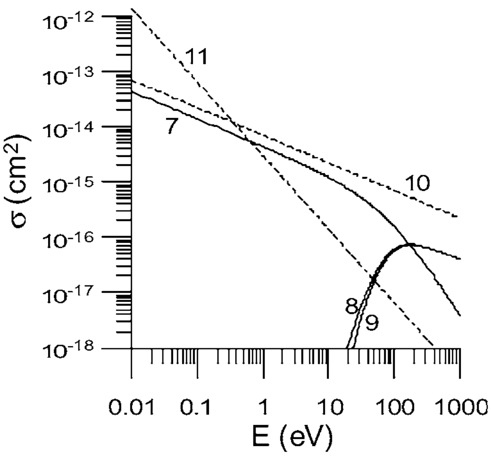

Fig. 2. Cross-sections of the ArH^+ reactions with Ar atoms (solid lines) and H_2 molecules (dashed lines) taken into account in the ArH^+ Monte Carlo model. The numbers of the curves correspond to the numbers in the text.

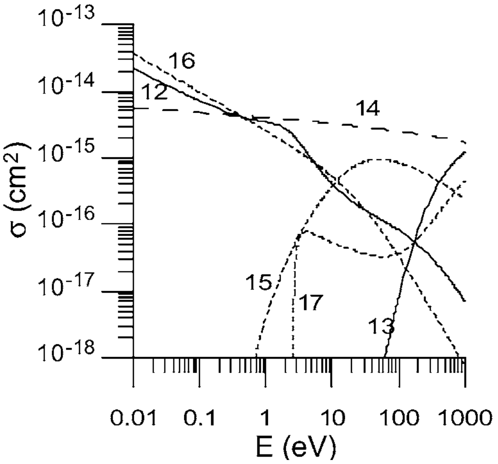

Fig. 3. Cross-sections of the H^+ reactions with Ar atoms (solid lines), H atoms (long dashed lines) and H_2 molecules (short dashed lines) taken into account in the H^+ Monte Carlo model. The numbers of the curves correspond to the numbers in the text.

figures correspond to the numbers in the following summary. The equations of the following reactions can be found below, in Table 1.

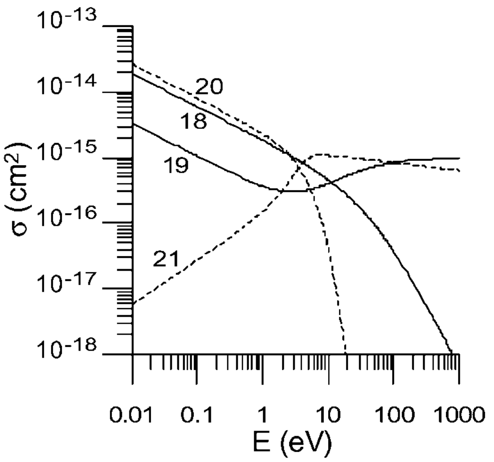

Fig. 4. Cross-sections of the H_2^+ reactions with Ar atoms (solid lines) and H_2 molecules (dashed lines) taken into account in the H_2^+ Monte Carlo model. The numbers of the curves correspond to the numbers in the text.

Ar^+ model	(1)	Elastic (isotropic) scattering with Ar [45]
	(2)	Elastic backward scattering (i.e. charge transfer) with Ar [45]
	(3)	Ionization of Ar [46]
	(4)	Excitation of Ar to the metastable levels [46]
	(5)	H-atom transfer with H_2 [47]
	(6)	Asymmetric charge transfer with H_2 [47]
ArH^+ model	(7)	Elastic scattering with Ar [48]
	(8)	Collision-induced dissociation of Ar, yielding Ar and H^+ [48]
	(9)	Collision-induced dissociation of Ar, yielding Ar^+ and H [48]
	(10)	Elastic scattering with H_2 [48]
	(11)	Proton transfer with H_2 [48]
H^+ model	(12)	Elastic scattering with Ar [48,49]
	(13)	Asymmetric charge transfer with Ar [47]
	(14)	Symmetric charge transfer with H [50]
	(15)	Total vibrational excitation of H_2 [51,52]
	(16)	Elastic scattering with H_2 [51,52]
	(17)	Asymmetric charge transfer with H_2 [51,52]
H_2^+ model	(18)	Proton transfer with Ar [47,48]
	(19)	Asymmetric charge transfer with Ar [47,48]
	(20)	Proton transfer with H_2 [51,52]
	(21)	Symmetric charge transfer with H_2 [51,52]
H_3^+ model	(22)	Elastic scattering with Ar [30,47,48]
	(23)	Proton transfer with Ar [30,47,48]
	(24)	Charge transfer + dissociation with Ar [30,47,48]
	(25)	Collision-induced dissociation with Ar, yielding H^+ and H_2 [30,47,48]
	(26)	Collision-induced dissociation with Ar, yielding H_2^+ and H [30,47,48]
	(27)	Elastic scattering with H_2 [31,48,51]
	(28)	Proton transfer with H_2 [31,48,51]
	(29)	Proton transfer + dissociation of H_2, yielding H_2 and H^+ [31,48,51]
	(30)	Proton transfer + dissociation of H_2, yielding H_2^+ and H [31,48,51]
	(31)	Charge transfer with H_2 + dissociation [31,48,51]
	(32)	Collision-induced dissociation with H_2, yielding H_2^+ and H [31,48,51]
	(33)	Collision-induced dissociation with H_2, yielding H^+ and H_2

		[31,48,51]
	(34)	Collision-induced dissociation with H_2, yielding H^+ and 2 H [31,48,51]
Fast Ar model	(35)	Elastic scattering with Ar [45]
	(36)	Ionization of Ar [46]
	(37)	Excitation of Ar to the metastable levels [46]

Some reactions, such as elastic scattering (including symmetric charge transfer), do not result in the creation of new species; they only change the energy and direction of the ions and atoms. However, most other reactions, such as proton transfer, asymmetric charge transfer, collision-induced dissociation, etc. lead to the destruction of the ions, and the formation of new types of ions and/or neutrals. These created species are also followed in the Monte Carlo models (for the ions and the fast Ar atoms), as well as in the fluid models (for the ions, the H atoms and H_2 molecules; see below).

Reactions 3 and 36, i.e. fast Ar^+ ion and Ar atom impact ionization, give rise to a new electron and an (additional) Ar^+ ion; the latter is also followed in the Ar^+ Monte Carlo model, whereas the electron is followed in the electron Monte Carlo model (see below). The rates of reactions 4 and 37, i.e. fast Ar^+ ion and Ar atom impact excitation to the Ar metastable level, are used in the Ar metastable model, to calculate the metastable density (see below).

All the ions which enter the CDS from the NG, as well as the ones created from collisions of the other species in the CDS are followed, until they are destroyed by chemical reactions or until they bombard the cathode (or the other cell walls), where they are assumed to be reflected as neutrals. The Ar^+ ions (as well as the Ar atoms) are reflected for 100% as neutral Ar atoms, with a fraction of their initial kinetic energy. It has been shown, for different gas (ion and atom)+metal combinations, that the fraction of energy deposited at the walls increases with the kinetic energy of the incoming particles [53,54]. The fraction of energy deposited on a copper surface as a function of incoming Ar ion and atom energy is adopted

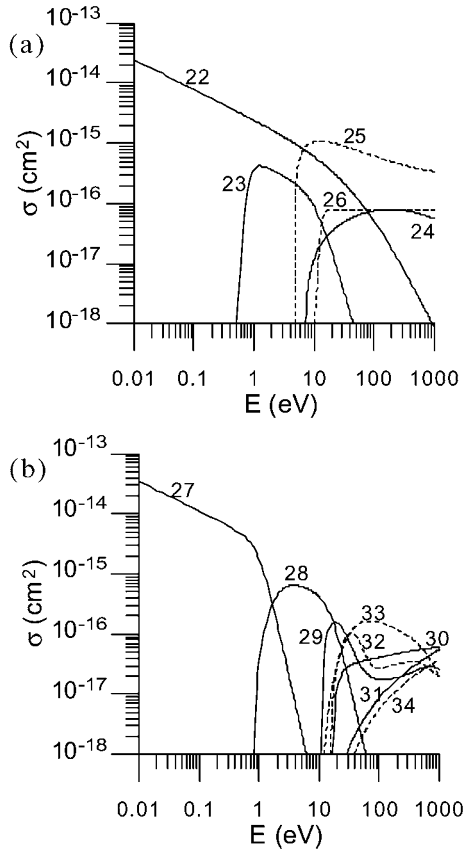

Fig. 5. Cross-sections of the H_3^+ reactions with Ar atoms (a) and H_2 molecules (b) taken into account in the H_3^+ Monte Carlo model. The numbers of the curves correspond to the numbers in the text. In both figures (a) and (b) the collision-induced dissociation reactions (either with Ar or with H_2) are presented with dashed lines, whereas all other reactions are presented with solid lines.

from Donko [55]. The reflection yield of H^+ ions as H atoms is assumed to be 0.6, independent of the ion energy [56]. In accordance with Petrovic et al. [56] we also assumed that the reflection yield of H_2^+, H_3^+ and ArH^+ ions under the form of H atoms is 1.2, 1.8 and 0.6, respectively. The H atoms are not followed with a MC algorithm, but their production rate due to reflection is used as an input in the H–H_2 fluid model (see below).

The fast Ar atoms created: (i) by neutralized reflection at the walls of the Ar^+ ions; (ii) by collisions of the various ions in the CDS; or (iii) from other fast Ar atoms by elastic collisions in

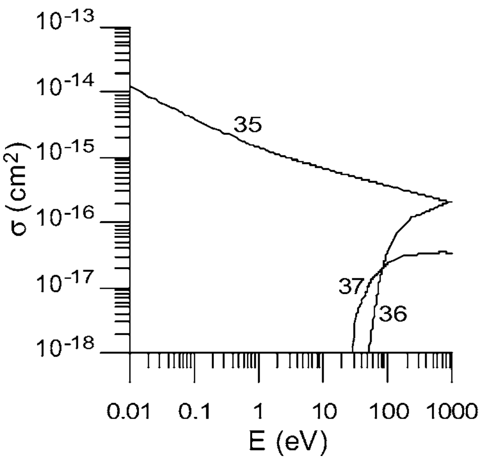

Fig. 6. Cross-sections of the Ar^0 reactions with Ar atoms taken into account in the Ar^0 Monte Carlo model. The numbers of the curves correspond to the numbers in the text.

the plasma or reflection at the walls, are followed with the Monte Carlo method, until their energy drops below 1 eV, because then they are not assumed to be 'fast' anymore.

2.2. Monte Carlo model for the electrons

The electrons start at the cathode, produced by secondary electron emission. It has been demonstrated [57] for Ar^+ ion and Ar atom bombardment on a variety of cathode surfaces that the secondary electron emission yields vary with incoming energy of the bombarding species, and are also strongly dependent on the surface condition. More specifically, a subdivision has been made between values obtained for clean surfaces (by sputtering under vacuum conditions) or dirty (gas covered) surfaces [57]. Similar differences also apply to the bombardment of hydrogen species on clean or dirty surfaces, e.g. Ray et al. [58] and Winter et al. [59]. However, in a previous paper [60] we have found for the conditions under study here (1000 V, 0.56 torr, a few mA, analytical glow discharge cell), that the different values for the secondary electron emission yields for clean and dirty surfaces, at least for Ar ion and atom bombardment, had only a minor effect on the final calculation results. Therefore, we will assume in this paper that our cathode is sufficiently cleaned by sputtering [60], to be able to use the values reported for clean surfaces. The emission yields for Ar ion and atom bombardment, as a function of incoming energy, are adopted from [57], whereas the values for H^+, H_2^+ and H_3^+ ions are taken from [59]. These values are actually for a clean gold surface, but it has been demonstrated [57] that the secondary electron emission yields are similar for different metal surfaces; hence, we use them also for a copper surface. It is stated [59] that there is no potential electron ejection for the hydrogen ions, i.e. no energy-independent yield at low energy. The data reported in Winter et al. [59] for H^+, H_2^+ and H_3^+ ions show a very similar behavior as a function of ion energy; so we have fitted them to the same analytical expression [48]. Finally, for ArH^+ bombardment, it is also assumed that potential (Auger) ejection is not important, because of the small amount of internal energy available, due to the large proton affinity for Ar [48]. Hence, only kinetic ejection plays a role. Note, that potential electron ejection occurs due to the internal (potential) energy of the bombarding particles, whereas kinetic ejection is caused by the kinetic energy of the bombarding particles. We assume that the secondary electron emission yield of ArH^+ is equal to the sum of Ar atom bombardment (for an energy equal to 40/41 of the ArH^+ energy) and H^+ ion bombardment (for an energy equal to 1/41 of the ArH^+ energy). This is based on the assumption that by hitting the surface ArH^+ is dissociated into Ar and H^+, which divide the initial energy corresponding to their mass, after which they independently liberate electrons, according to what individual Ar atoms and H^+ ions would do. This gives the following formulas for the secondary electron emission yields as a function of bombarding energy [48,57,59]:

Ar^+ ions: if $E \leq 500$ eV: $\gamma_{Ar^+} = 0.07$

$$\text{if} \quad E > 500 \text{ eV:} \quad \gamma_{Ar^+} = 0.07 + \frac{10^{-5}(E-500)^{1.2}}{1+\left(\frac{E}{70000}\right)^{0.7}}$$

Ar atoms: if $E \leq 500$ eV: $\gamma_{Ar^0} = 0$

if $E > 500$ eV: $\gamma_{Ar^0} \dfrac{10^{-5}(E-500)^{1.2}}{1+\left(\dfrac{E}{70000}\right)^{0.7}}$

H^+, H_2^+, H_3^+ ions: $\gamma_H = 10^{-5} E^{1.3}$

ArH^+ ions: if $E \leq 500$ eV:

$$\gamma_{ArH^+} = 10^{-5}\left(\frac{1}{41}E\right)^{1.3}$$

if $E > 500$ eV:

$$\gamma_{ArH^+} = \frac{10^{-5}\left(E\dfrac{40}{41} - 500\right)^{1.2}}{1+\left(\dfrac{E\dfrac{40}{41}}{70000}\right)^{0.7}} + 10^{-5}\left(\frac{1}{41}E\right)^{1.3}$$

These different secondary electron emission yields are plotted against ion or atom energy in Fig. 7a. It is clear that, at the typical ion and atom energies under consideration (10–100 eV), the Ar ions will play a dominant role in secondary electron emission, if the cathode surface is considered to be clean. Indeed, the other species are assumed not to give rise to potential ejection, and kinetic ejection starts only playing a role at high enough energies (several hundred eV). Note, however, that this picture would be different for dirty surfaces, where the H_2 species and the fast Ar atoms have somewhat higher secondary electron emission yields in the typical energy range of interest. This will, of course, affect the quantitative results of the model (i.e. the flux of electrons, and hence the ionization rates, densities of the plasma species, and the electrical current). However, this paper focuses on the qualitative predictions (and orders of magnitude) of the densities of the various species and the importance of the different production and loss mechanisms, and for this purpose, it is not so important whether secondary electron emission yields for clean or dirty surfaces are used.

The electrons emitted from the cathode are accelerated in the CDS by the strong electric field, and they are also subject to collisions. The collision processes taken into account in this model, with the references of the cross-sections, are:

(38) Elastic scattering with Ar [57]
(39) Ionization of Ar [57]
(40) Total excitation of Ar [57]
(41) Ionization from the Ar metastable levels [61]
(42) Total excitation from the Ar metastable levels [62]
(43) Elastic scattering with H_2 [63]
(44) Total vibrational excitation of H_2 [63]
(45) Total electron excitation of H_2 to the singlet states [63]
(46) Total electron excitation of H_2 to the triplet states, followed by dissociation [63]
(47) Ionization of H_2 [63]
(48) Dissociative ionization of H_2 [64]
(49) Total excitation of H [50]
(50) Ionization of H [50]

The corresponding cross-sections as a function of electron energy are depicted in Fig. 7b,c (for the collisions with Ar ground state or metastable atoms and with H_2 or H, respectively). The numbers given in these figures correspond to the above numbers.

The elastic scattering reactions (no. 38 and 43) lead to a change in direction of the electrons but nearly no change in energy, due to the large difference in mass of electrons and Ar atoms or H_2 molecules. The electron impact ionization of different species (Ar ground state or metastable atoms, H_2 molecules or H atoms; i.e. no. 39, 41, 47, 48 and 50) give rise to a new electron (which is also followed in this electron Monte Carlo model) and an ion (Ar^+, H_2^+, or H^+). These ions are also followed in the ion Monte Carlo models described above. Two kinds of electron impact excitation are considered in the model: total vibrational excitation of H_2 molecules (no. 44, which in our model leads only to a change in energy and direction of the electrons, because the vibrationally excited H_2 molecules are not explicitly followed in the model); and total electronic excitation (no. 40, 42, 45, 46 and 49). Reaction no. 40 stands for total electronic excitation of Ar (i.e. summed over all Ar excited levels), but the excitation to the Ar metastable levels is also explicitly described in this model, because it is necessary as input for the

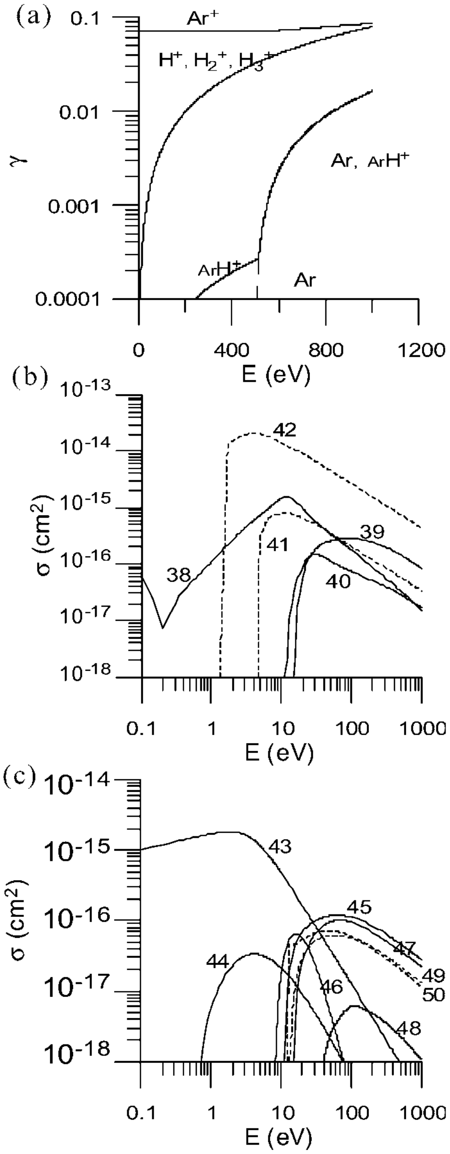

Fig. 7. Secondary electron emission yields by Ar^+ ions, H^+, H_2^+ and H_3^+ ions, ArH^+ ions and Ar^0 atoms, as a function of the ion and atom energy (a), and cross-sections of the electron reactions with Ar atoms (b: solid lines), Ar metastable atoms (b: dashed lines), H_2 molecules (c: solid lines) and H atoms (c: dashed lines) taken into account in the electron Monte Carlo model. The numbers of the curves in figures (b) and (c) correspond to the numbers in the text.

Ar metastable model (see below). Similarly, electron impact ionization and excitation from the Ar metastable level (reactions no. 41 and 42) are included in the MC model, because they are also used as input in the Ar metastable model.

Electronic excitation of the H_2 molecules can lead either to singlet or triplet states. In our model, we use only two electronic excitation cross-sections for H_2, i.e. for the sum over all singlet states and over all triplet states. It is generally known that excitation to the triplet states leads to dissociation of the H_2 molecule. Indeed, all triplet states will radiate to the lowest triplet H_2 state (b $^3\Sigma_u^+$) [65], which is formed by two H ground state atoms, in which one electron is in a binding orbital and the other in an antibinding orbital. This state is repulsive, and will consequently dissociate into two H atoms. Moreover, we assume that 15% of the singlet excitation also leads to dissociation, based on the cross-sections of photon emission for the Ly-α, Ly-β, H-α, H-β, H-γ, H-δ lines and the production of metastable H(2s) atoms [64]. Therefore, the total dissociation rate of H_2 due to electron impact excitation is calculated in our model as the sum of the total triplet excitation rate + 15% of the total singlet excitation rate. Finally, rotational excitation of H_2 is neglected in the model because: (i) the energy loss is small, and it has no effect on the electron energy distribution function; and (ii) the rotationally excited H_2 molecules are not considered in the model.

The electrons are followed in the Monte Carlo model during successive time-steps, until they bombard the walls (where they can be reflected, cause secondary electron emission, or become absorbed), or until their energy in the NG drops below 0.5 eV, which is the threshold for inelastic collisions with H_2 (i.e. vibrational excitation; see Fig. 7c). Note that in our previous electron Monte Carlo model for Ar, the electrons were followed till an energy of 11.55 eV (i.e. the threshold for excitation of Ar) [66]. In order to limit the calculation time, when a large number of slow electrons has to be simulated, a variable time-step (depending on the electron energy) is used to calculate the electron trajectories in the negative glow.

Table 1
Production and loss processes for the different species, taken into account in the electron-ion fluid model

No.	Reaction	Name	Model used to treat this process
Production of electrons			
3	$Ar^+ + Ar \rightarrow Ar^+ + Ar^+ + e^-$	Ionization of Ar	Ar^+ MC model (CDS)
36	Fast $Ar + Ar \rightarrow$ fast $Ar + Ar^+ + e^-$	Ionization of Ar	Fast Ar MC model (CDS)
39	$e^- + Ar \rightarrow e^- + Ar^+ + e^-$	Ionization of Ar	Electron MC model
41	$e^- + Ar_m{}^* \rightarrow e^- + Ar^+ + e^-$	Ionization of Ar metast.	Electron MC model
47	$e^- + H_2 \rightarrow e^- + H_2^+ + e^-$	Ionization of H_2	Electron MC model
48	$e^- + H_2 \rightarrow e^- + H^+ + H + e^-$	Dissoc. ionization of H_2	Electron MC model
50	$e^- + H \rightarrow e^- + H^+ + e^-$	Ionization of H	Electron MC model
Loss of electrons			
51	$e^- + ArH^+ \rightarrow Ar + H$	Recombination	Fluid model: $k = 10^{-7}$ cm^3 s^{-1} [10]
52	$e^- + H_2^+ \rightarrow H + H$	Recombination	Fluid model: $k = 10^{-7}$ cm^3 s^{-1} [10]
53	$e^- + H_3^+ \rightarrow H + H + H$ or $H_2 + H$	Recombination	Fluid model: $k = 10^{-7}$ cm^3 s^{-1} [39,44]
Production of Ar^+ ions			
3	$Ar^+ + Ar \rightarrow Ar^+ + Ar^+ + e^-$	Ionization	Ar^+ MC model (CDS)
9	$ArH^+ + Ar \rightarrow$ fast $Ar^+ + H + Ar$	Collision-induced dissoc.	ArH^+ MC model (CDS)
13	$H^+ + Ar \rightarrow$ fast $H + Ar^+$	Charge transfer	H^+ MC model (CDS)
19	$H_2^+ + Ar \rightarrow$ fast $H_2 + Ar^+$	Charge transfer	H_2^+ MC model (CDS) fluid model: $k = 2.2 \times 10^{-10}$ cm^3 s^{-1}
24	$H_3^+ + Ar \rightarrow$ fast $H_2 +$ fast $H + Ar^+$	Charge transfer + dissoc.	H_3^+ MC model (CDS)
36	Fast $Ar + Ar \rightarrow$ fast $Ar + Ar^+ + e^-$	Ionization	Fast Ar MC model (CDS)
39	$e^- + Ar \rightarrow e^- + Ar^+ + e^-$	Ionization	Electron MC model
41	$e^- + Ar_m{}^* \rightarrow e^- + Ar^+ + e^-$	Ionization	Electron MC model
Loss of Ar^+ ions			
5	$Ar^+ + H_2 \rightarrow ArH^+ + H$	H-atom transfer	Ar^+ MC model (CDS) fluid model: $k = 6 \times 10^{-10}$ cm^3 s^{-1}
6	$Ar^+ + H_2 \rightarrow$ fast $Ar + H_2^+$	Charge transfer	Ar^+ MC model (CDS) fluid model: $k = 8 \times 10^{-11}$ cm^3 s^{-1}
Production of ArH^+ ions			
5	$Ar^+ + H_2 \rightarrow ArH^+ + H$	H-atom transfer	Ar^+ MC model (CDS) fluid model: $k = 6 \times 10^{-10}$ cm^3 s^{-1}
18	$H_2^+ + Ar \rightarrow H + ArH^+$	Proton transfer	H_2^+ MC model (CDS) fluid model: $k = 1.7 \times 10^{-9}$ cm^3 s^{-1}
23	$H_3^+ + Ar \rightarrow$ fast $H_2 +$ slow ArH^+	Proton transfer	H_3^+ MC model (CDS)
Loss of ArH^+ ions			
51	$e^- + ArH^+ \rightarrow Ar + H$	Recombination	Fluid model: $k = 10^{-7}$ cm^3 s^{-1} [10]
8	$ArH^+ + Ar \rightarrow$ fast $Ar + H^+ + Ar$	Collision-induced dissoc.	ArH^+ MC model (CDS)
9	$ArH^+ + Ar \rightarrow$ fast $Ar^+ + H + Ar$	Collision-induced dissoc.	ArH^+ MC model (CDS)
11	$ArH^+ + H_2 \rightarrow$ fast $Ar + H_3^+$	Proton transfer	ArH^+ MC model (CDS) fluid model: $k = 1.5 \times 10^{-9}$ cm^3 s^{-1} [44]
Production of H^+ ions			
8	$ArH^+ + Ar \rightarrow$ fast $Ar + H^+ + Ar$	Collision-induced dissoc.	ArH^+ MC model (CDS)
25	$H_3^+ + Ar \rightarrow$ fast $H^+ +$ fast $H_2 +$ slow Ar	Collision-induced dissoc.	H_3^+ MC model (CDS)
29	$H_3^+ + H_2 \rightarrow$ fast $H_2 +$ slow $H_2 +$ slow H^+	Proton transfer + dissoc.	H_3^+ MC model (CDS)
33	$H_3^+ + H_2 \rightarrow$ fast $H^+ +$ fast $H_2 +$ slow H_2	Collision-induced dissoc.	H_3^+ MC model (CDS)
34	$H_3^+ + H_2 \rightarrow$ fast $H^+ + 2$ fast $H +$ slow H_2	Collision-induced dissoc.	H_3^+ MC model (CDS)
48	$e^- + H_2 \rightarrow e^- + H^+ + H + e^-$	Dissociative ionization	Electron MC model
50	$e^- + H \rightarrow e^- + H^+ + e^-$	Ionization	Electron MC model

Table 1 *(Continued)*

No.	Reaction	Name	Model used to treat this process
Loss of H^+ ions			
13	$H^+ + Ar \rightarrow$ fast $H + Ar^+$	Charge transfer	H^+ MC model (CDS)
17	$H^+ + H_2 \rightarrow$ fast $H + H_2^+$	Charge transfer	H^+ MC model (CDS)
Production of H_2^+ ions			
6	$Ar^+ + H_2 \rightarrow$ fast $Ar + H_2^+$	Charge transfer	Ar^+ MC model (CDS) fluid model: $k=8\times10^{-11}$ cm^3 s^{-1}
17	$H^+ + H_2 \rightarrow$ fast $H + H_2^+$	Charge transfer	H^+ MC model (CDS)
26	$H_3^+ + Ar \rightarrow$ fast $H_2^+ +$ fast $H +$ slow Ar	Collision-induced dissoc.	H_3^+ MC model (CDS)
30	$H_3^+ + H_2 \rightarrow$ fast $H_2 +$ slow $H +$ slow H_2^+	Proton transfer + dissoc.	H_3^+ MC model (CDS)
31	$H_3^+ + H_2 \rightarrow$ fast $H_2 +$ fast $H +$ slow H_2^+	Charge transfer + dissoc.	H_3^+ MC model (CDS)
32	$H_3^+ + H_2 \rightarrow$ fast $H_2^+ +$ fast $H +$ slow H_2	Collision-induced dissoc.	H_3^+ MC model (CDS)
47	$e^- + H_2 \rightarrow e^- + H_2^+ + e^-$	Ionization	Electron MC model
Loss of H_2^+ ions			
52	$e^- + H_2^+ \rightarrow H + H$	Recombination	Fluid model: $k=10^{-7}$ cm^3 s^{-1} [10]
18	$H_2^+ + Ar \rightarrow H + ArH^+$	Proton transfer	H_2^+ MC model (CDS) fluid model: $k=1.7\times10^{-9}$ cm^3 s^{-1}
19	$H_2^+ + Ar \rightarrow$ fast $H_2 + Ar^+$	Charge transfer	H_2^+ MC model (CDS) fluid model: $k=2.2\times10^{-10}$ cm^3 s^{-1}
20	$H_2^+ + H_2 \rightarrow H_3^+ + H$	Proton transfer	H_2^+ MC model (CDS) fluid model: $k=2\times10^{-9}$ cm^3 s^{-1}
Production of H_3^+ ions			
11	$ArH^+ + H_2 \rightarrow$ fast $Ar + H_3^+$	Proton transfer	ArH^+ MC model (CDS) fluid model: $k=1.5\times10^{-9}$ cm^3 s^{-1}
20	$H_2^+ + H_2 \rightarrow H + H_3^+$	Proton transfer	H_2^+ MC model (CDS) fluid model: $k=2\times10^{-9}$ cm^3 s^{-1}
Loss of H_3^+ ions			
53	$e^- + H_3^+ \rightarrow H + H + H$ or $H_2 + H$	Recombination	Fluid model: $k=10^{-7}$ cm^3 s^{-1} [39,44]
23	$H_3^+ + Ar \rightarrow$ fast $H_2 +$ slow ArH^+	Proton transfer	H_3^+ MC model (CDS)
24	$H_3^+ + Ar \rightarrow$ fast $H_2 +$ fast $H +$ slow Ar^+	Charge transfer + dissoc.	H_3^+ MC model (CDS)
25	$H_3^+ + Ar \rightarrow$ fast $H^+ +$ fast $H_2 +$ slow Ar	Collision-induced dissoc.	H_3^+ MC model (CDS)
26	$H_3^+ + Ar \rightarrow$ fast $H_2^+ +$ fast $H +$ slow Ar	Collision-induced dissoc.	H_3^+ MC model (CDS)
29	$H_3^+ + H_2 \rightarrow$ fast $H_2 +$ slow $H_2 +$ slow H^+	Proton transfer + dissoc.	H_3^+ MC model (CDS)
30	$H_3^+ + H_2 \rightarrow$ fast $H_2 +$ slow $H +$ slow H_2^+	Proton transfer + dissoc.	H_3^+ MC model (CDS)
31	$H_3^+ + H_2 \rightarrow$ fast $H_2 +$ fast $H +$ slow H_2^+	Charge transfer + dissoc.	H_3^+ MC model (CDS)
32	$H_3^+ + H_2 \rightarrow$ fast $H_2^+ +$ fast $H +$ slow H_2	Collision-induced dissoc.	H_3^+ MC model (CDS)
33	$H_3^+ + H_2 \rightarrow$ fast $H^+ +$ fast $H_2 +$ slow H_2	Collision-induced dissoc.	H_3^+ MC model (CDS)
34	$H_3^+ + H_2 \rightarrow$ fast $H^+ + 2$ fast $H +$ slow H_2	Collision-induced dissoc.	H_3^+ MC model (CDS)

The numbers in column 1 correspond to the reactions given in Sections 2.1 and 2.2, with a few exceptions (i.e. ion-electron recombination, numbers 51–53, which was not simulated in the MC models). If the collision process is (also) treated in the fluid model, the rate coefficients, either calculated from the cross-sections in Figs. 1–7, or adopted from the literature, are also given.

2.3. Fluid model for electrons, Ar^+, ArH^+, H^+, H_2^+ and H_3^+ ions

The various ions and the electrons are not only followed with Monte Carlo models, as described above, but they are also treated with a fluid model. The latter model consists of continuity (balance) equations and transport equations (based on diffusion and migration) for all species, coupled to Poisson's equation for the self-consistent calculation of the electric field distribution. Hence, both the electrons and the different ions are treated simultaneously in two models: the fluid model is used to calculate the species densities and fluxes, in accordance with the self-consistently calculated electric field distribution; whereas the Monte Carlo codes serve to calculate the collision processes and hence the production and loss rates of the various species. The latter are much more accurately calculated with a Monte Carlo method, which treats the species explicitly and on the lowest microscopic level. The production and loss rates calculated in the Monte Carlo codes are then used as input for the balance equations in the fluid model. Because the Monte Carlo models also calculate the energy of the various ions and the electrons, there are no energy balance equations included in the fluid model. Indeed, the energy is much more accurately calculated in the Monte Carlo models than it would be in the fluid code through energy balance equations.

As mentioned above, the fluid model consists of a set of continuity and transport equations (12 in total, i.e. for the five ions and for the electrons):

$$\frac{\partial n_x}{\partial t}+\overline{\nabla}\cdot\overline{j_x}=R_{\mathrm{prod},x}-R_{\mathrm{loss},x}$$

$$\overline{j_x}=\pm\mu_x n_x\overline{E}-D_x\overline{\nabla}n_x$$

where x stands for every type of ion (Ar^+, ArH^+, H^+, H_2^+ and H_3^+) or for the electrons, n and j denote the species density and flux, R_{prod} and R_{loss} are the species total production and loss rates, μ and D are the species mobility and diffusion coefficients, and E is the electric field distribution. In the transport equation, a positive sign in the migration term is used for the ions, whereas a negative sign is used for the electrons. The mobility and diffusion coefficients assumed in the model for the Ar ions and electrons were the same as used in our previous models (see e.g. Bogaerts et al. [66]), i.e. for a pure Ar discharge. Indeed, the 1% H_2 admixture to the Ar gas will have only a minor effect on the transport coefficients. The diffusion coefficients for the ArH^+, H^+, H_2^+ and H_3^+ ions in Ar/H_2 are calculated with a formula of the rigid sphere model for a mixture of two chemical species [67]. The mobilities of ArH^+ and H_3^+ ions in Ar/H_2 are adopted from Mcafee et al. [68]. In view of the lack of calculations or measurements of ion transport for H^+ and H_2^+ in Ar, we will assume that the mobilities of H^+ and H_2^+ are the same as for H_3^+. In principle, the mobilities of H^+, H_2^+ and H_3^+ ions should be different, because they have different mass and different collision frequency. However, as will be shown later, the role of H^+ and H_2^+ ions in the plasma is negligible, so that this assumption has no effect on the overall calculation results.

The different production and loss processes taken into account for the various ions and for the electrons, are summarized in Table 1. The numbers in the first column correspond to the reactions given in Sections 2.1 and 2.2, with a few exceptions (i.e. for the reactions that are not treated in the Monte Carlo models). As follows from this table, the production and loss rates are mostly calculated in the Monte Carlo models, i.e. in the entire discharge for the electron-induced processes, and in the CDS for the ion-induced processes. However, in addition, some of the ion-induced chemical reactions are also treated in the fluid model itself, i.e. when the cross-section is high at thermal energy, so that the process can occur with thermal ions in the NG. In the latter case, some additional production and loss rates are calculated based on the densities of the collision partners multiplied with the rate coefficients. The latter are calculated from the cross-sections at thermal energy (see Figs. 1–7). The values calculated in this way are also presented in Table 1, and they appear to be in good agreement with rate coefficients found in the literature [32,44,69]. Finally, electron ion recombination, which was not considered in the MC models because it applies to thermal electrons, is also treated in the fluid model. Only recombination with the molecular ions (ArH^+, H_2^+ and H_3^+) is taken into account. Indeed, recombination with atomic ions (Ar^+ and H^+) is negligible because of too low rate coefficients. The recombination rates were also calculated based on the rate coefficients and the densities of the reacting species. The rate coefficients used in our model, as well as the references where the values are adopted from, are given in Table 1 as well.

Six continuity equations and six transport equations are constructed in this way, and they are coupled to Poisson's equation, to calculate the electric field distribution from the different ion and the electron densities:

$$\overline{\nabla} \cdot \overline{E} = \frac{e}{\varepsilon_0}(n_{\mathrm{Ar}^+} + n_{\mathrm{ArH}^+} + n_{\mathrm{H}^+} + n_{\mathrm{H_2}^+} + n_{\mathrm{H_3}^+} - n_{\mathrm{e}})$$

The set of coupled differential equations is solved with the Scharfetter–Gummel exponential scheme [66,70–72].

2.4. Fluid model for H atoms and H_2 molecules

The H atoms and H_2 molecules are also described with a set of two coupled continuity (balance) equations, with different production and loss rates, as well as with two transport equations (determined by diffusion). These four equations could in principle be coupled with the continuity and transport equations of the various ions and the electrons, in the ion-electron fluid model. However, the time-step in the ion-electron fluid model had to be much smaller than for the neutral species, due to the severe coupling with Poisson's equation. Therefore, we have chosen not to further increase the calculation time, and to decouple the fluid model for the neutral species (H and H_2) from the ion-electron fluid model.

The continuity and transport equations for the H atoms and H_2 molecules have a form similar to above (except that transport is now only dictated by diffusion):

$$\frac{\partial n_x}{\partial t} + \overline{\nabla} \cdot \overline{j_x} = R_{\mathrm{prod},x} - R_{\mathrm{loss},x}$$

$$\overline{j_x} = -D_x \overline{\nabla} n_x$$

The different production and loss processes for the H atoms and H_2 molecules are summarized in Table 2. Again, most production and loss rates are calculated with the MC models of ions and electrons, and the numbers in the first column correspond to the numbers given in Sections 2.1 and 2.2. In addition, the ion-induced reactions with high cross-sections at thermal energy (so that the reactions can occur in the NG, with thermal ions) are also treated in the H–H_2 fluid model, based on the rate coefficients and the densities of the reacting species, in analogy to the above electron-ion fluid model. The corresponding reaction rate coefficients were given already in Table 1. Some reactions (i.e. no. 34, 46, 52, 53 and 54) yield the formation of two H-atoms. Hence, the production rate of H-atoms is then equal to twice the reaction rate. Similarly, reaction 53 gives rise to the formation of half a H_2 molecule (assuming that the two possible reaction channels have equal probability); hence the production rate of the H_2 molecules is then determined by half the reaction rate.

Reaction no. 54 did not occur in any of the tables above. Indeed, it is not treated in any of the MC models, neither in the electron-ion fluid model, because it is induced by Ar metastable atoms. In analogy to the thermal ion-induced reactions, the rate of this reaction is calculated based on the Ar metastable density calculated in the metastable model (see below) and the H_2 density, multiplied with the corresponding rate coefficient. In the literature, this rate coefficient is presented separately for the two metastable 4s levels [32,73–75]. In the Ar metastable model used for the present investigation [76], we consider, however, only one type of metastable atoms, combining the two metastable 4s levels in a collective level lying at 11.55 eV. This is a reasonable assumption, because the two metastable levels lie close to each other, and the 4s $[3/2]_2$ metastable level (also denoted as $^3P_2$ level) lying at 11.55 eV, has a clearly higher population density than the other metastable level [77]. From the level populations of the individual 4s metastable levels calculated in [77], we roughly calculated their 'fractional population' and multiplied the latter with the individual rate coefficients of reaction no. 54, found in the literature. This gives us an overall rate coefficient of approximately 7×10^{-11} cm^3 s^{-1} (see Table 2), which subsequently has to be combined with the metastable atom density calculated in the metastable model (see below). The importance of this reaction for the dissociation of H_2 molecules into H atoms has been demonstrated in the literature by the strong continuum emission in the spectral range of 220–440 nm, in Ar/H_2 glow discharges [4–6,29]. This continuum is considered to be the result of the sequence [4–6,29,78]:

Table 2
Production and loss processes taken into account in the H–H_2 fluid model

No.	Reaction	Name	Model used to treat this process
Production of H atoms			
5	$Ar^+ + H_2 \rightarrow ArH^+ + H$	H-atom transfer	Ar^+ MC model (CDS) H–H_2 fluid model
9	$ArH^+ + Ar \rightarrow$ fast $Ar^+ + H + Ar$	Collision-induced dissoc.	ArH^+ MC model (CDS)
13	$H^+ + Ar \rightarrow$ fast $H + Ar^+$	Charge transfer	H^+ MC model (CDS)
17	$H^+ + H_2 \rightarrow$ fast $H + H_2^+$	Charge transfer	H^+ MC model (CDS)
18	$H_2^+ + Ar \rightarrow H + ArH^+$	Proton transfer	H_2^+ MC model (CDS) H–H_2 fluid model
20	$H_2^+ + H_2 \rightarrow H + H_3^+$	Proton transfer	H_2^+ MC model (CDS) H–H_2 fluid model
24	$H_3^+ + Ar \rightarrow$ fast H_2 + fast H + slow Ar^+	Charge transfer + dissoc.	H_3^+ MC model (CDS)
26	$H_3^+ + Ar \rightarrow$ fast H_2^+ + fast H + slow Ar	Collision-induced dissoc.	H_3^+ MC model (CDS)
30	$H_3^+ + H_2 \rightarrow$ fast H_2 + slow H + slow H_2^+	Proton transfer + dissoc.	H_3^+ MC model (CDS)
31	$H_3^+ + H_2 \rightarrow$ fast H_2 + fast H + slow H_2^+	Charge transfer + dissoc.	H_3^+ MC model (CDS)
32	$H_3^+ + H_2 \rightarrow$ fast H_2^+ + fast H + slow H_2	Collision-induced dissoc.	H_3^+ MC model (CDS)
34	$H_3^+ + H_2 \rightarrow$ fast H^+ + 2 fast H + slow H_2	Collision-induced dissoc.	H_3^+ MC model (CDS) (2 H prod)
46	$e^- + H_2 \rightarrow e^- + H_2^*$ (t) $\rightarrow e^- + H + H$	Electron excit. + dissoc.	Electron MC model (2 H prod)
48	$e^- + H_2 \rightarrow e^- + H^+ + H + e^-$	Dissociative ionization	Electron MC model
51	$e^- + ArH^+ \rightarrow Ar + H$	Recombination	Ion-electron fluid model
52	$e^- + H_2^+ \rightarrow H + H$	Recombination	Ion-electron fluid model (2 H prod)
53	$e^- + H_3^+ \rightarrow H + H + H$ or $H_2 + H$	Recombination	Ion-electron fluid model (2 H prod)
54	$Ar_m^* + H_2 \rightarrow Ar + H + H$	Quenching + dissoc.	H–H_2 fluid model; $k = 7\times10^{-11}$ cm^3 s^{-1} [32,73–75] (2 H prod)
55	ArH^+ (at walls) $\rightarrow$ 0.6 H H^+ (at walls) $\rightarrow$ 0.6 H H_2^+ (at walls) $\rightarrow$ 1.2 H H_3^+ (at walls) $\rightarrow$ 1.8 H	Reflection at walls	ArH^+, H^+, H_2^+, H_3^+ MC models
Loss of H atoms			
50	$e^- + H \rightarrow e^- + H^+ + e^-$	Ionization	Electron MC model
56	$H + H(wall) \rightarrow H_2$	Recombination at walls	H–H_2 fluid model ($\gamma = 0.1$) [79]
Production of H_2 molecules			
19	$H_2^+ + Ar \rightarrow$ fast $H_2 + Ar^+$	Charge transfer	H_2^+ MC model (CDS) H–H_2 fluid model
23	$H_3^+ + Ar \rightarrow$ fast H_2 + slow ArH^+	Proton transfer	H_3^+ MC model (CDS)
24	$H_3^+ + Ar \rightarrow$ fast H_2 + fast H + slow Ar^+	Charge transfer + dissoc.	H_3^+ MC model (CDS)
25	$H_3^+ + Ar \rightarrow$ fast H^+ + fast H_2 + slow Ar	Collision-induced dissoc.	H_3^+ MC model (CDS)
29	$H_3^+ + H_2 \rightarrow$ fast H_2 + slow H_2 + slow H^+	Proton transfer + dissoc.	H_3^+ MC model (CDS)
33	$H_3^+ + H_2 \rightarrow$ fast H^+ + fast H_2 + slow H_2	Collision-induced dissoc.	H_3^+ MC model (CDS)
53	$e^- + H_3^+ \rightarrow H + H + H$ or $H_2 + H$	Recombination	Ion-elec. fluid model (0.5 H_2 prod.)
56	$H + H(wall) \rightarrow H_2$	Recombination at walls	H–H_2 fluid model ($\gamma = 0.1$) [79]
Loss of H_2 molecules			
5	$Ar^+ + H_2 \rightarrow ArH^+ + H$	H-atom transfer	Ar^+ MC model (CDS) H–H_2 fluid model
6	$Ar^+ + H_2 \rightarrow$ fast $Ar + H_2^+$	Charge transfer	Ar^+ MC model (CDS) H–H_2 fluid model
11	$ArH^+ + H_2 \rightarrow$ fast $Ar + H_3^+$	Proton transfer	ArH^+ MC model (CDS) H–H_2 fluid model

Table 2 *(Continued)*

No.	Reaction	Name	Model used to treat this process
17	$H^+ + H_2 \rightarrow \text{fast } H + H_2^+$	Charge transfer	H^+ MC model (CDS)
20	$H_2^+ + H_2 \rightarrow H_3^+ + H$	Proton transfer	H_2^+ MC model (CDS) H–H_2 fluid model
46	$e^- + H_2 \rightarrow e^- + H_2^*\ (t) \rightarrow e^- + H + H$	Electron excit. + dissoc.	Electron MC model
47	$e^- + H_2 \rightarrow e^- + H_2^+ + e^-$	Ionization	Electron MC model
48	$e^- + H_2 \rightarrow e^- + H^+ + H + e^-$	Dissociative ionization	Electron MC model
54	$Ar_m^* + H_2 \rightarrow Ar + H + H$	Quenching + dissoc.	H–H_2 fluid model; $k = 7 \times 10^{-11}$ cm^3 s^{-1} [32,73–75]

$$Ar_m^* + H_2(X^1\Sigma_g^+) \rightarrow Ar(^1S_0) + H_2(a^3\Sigma_g^+)$$
$$H_2(a^3\Sigma_g^+) \rightarrow H_2(b^3\Sigma_u^+) + h\nu \quad \text{(continuum)}$$
$$H_2(b^3\Sigma_u^+) \xrightarrow{\text{dissociation}} H + H$$

An alternative reaction path is the excitation into the triplet state by electron impact, followed also by dissociation (see above, reaction no. 46). However, in neon/H_2 mixtures, where excitation of the H_2 molecules by neon metastables is not possible, no significant continuum was observed under similar experimental conditions [6]. This suggests that electron impact excitation followed by dissociation (reaction 46) is probably less important than excitation by Ar metastables followed by dissociation (reaction 54).

Beside the chemical reactions taking place in the plasma, two processes occurring at the walls, might play an important role in determining the H and H_2 densities, i.e. reflection at the walls of ArH^+, H^+, H_2^+ and H_3^+ ions under the form of H atoms (reaction no. 55) and recombination of H atoms at the walls (which are assumed to be saturated with H atoms) into H_2 molecules (reaction no. 56). The first reaction is treated in the ion MC models (see above), yielding a production rate of H atoms, localized at the walls, which is used as input in the H–H_2 fluid model. The second reaction, which defines a loss of the H atoms and a formation of H_2 molecules, is treated in the H–H_2 fluid model itself, by using the appropriate boundary conditions in the balance equations of H atoms and H_2 molecules. The recombination coefficient of H-atoms (γ_{rec}) is found to be in the order of 0.1–0.25 for most metal surfaces [79]. For a copper surface, values were determined to vary between 0.1 and 0.14, for a wide range of surface temperatures (300–700 K) [37,79], indicating that the values are insensitive to the surface temperature in the range of measurements. We adopted a value of 0.1, which means that 10% of the H atoms arriving at the walls will recombine into H_2 molecules. The boundary condition at the cell walls is adopted from [80]:

$$\frac{1}{n}(\nabla n)_{\text{wall}} = -\frac{1}{\lambda}$$

Here λ is the 'linear extrapolation length', defined as:

$$\lambda = \varepsilon \lambda_m \frac{1+R}{1-R}$$

where ε is a coefficient varying between 0.67 and 0.71, depending weakly on the 'reflection coefficient' R (which is here related to the recombination coefficient), and λ_m is the diffusion mean free path ($=1/N\sigma_m$).

This wall recombination of H atoms is suggested to be the dominant production mechanism of H_2 molecules in Ar/H_2 supersonically expanding cascaded arc plasmas (where no H_2 molecules, but only Ar^+, Ar, H^+, H and electrons are assumed to leave the arc) [10]. Therefore, the above process is also taken into account in our model, although the discharge conditions under study in our work are completely different. Indeed, we assume that the 1% hydrogen is added in molecular form (hence no initial dissociation), and we expect that the final dissociation degree is also rather low.

2.5. Fluid model for the Ar metastable atoms

The models developed for the hydrogen species should also be coupled with a model for the Ar

Table 3
Production and loss processes taken into account in the Ar metastable model

No.	Reaction	Name	Model used to treat this process
Production of Ar metastable atoms			
40	$Ar+e^- \rightarrow Ar_m{}^* + e^-$	Elec. impact excitation	Electron MC model
4	$Ar+Ar^+ \rightarrow Ar_m{}^* + Ar^+$	Ar ion impact excitation	Ar^+ MC model (CDS)
37	$Ar+Ar_f^0 \rightarrow Ar_m{}^* + Ar_f^0$	Ar atom impact excitation	Ar^0 MC model (CDS)
57	$Ar^+ + e^- \rightarrow Ar_m{}^* + h\nu$	Radiative recombination	Ar metast. model; $k=10^{-11}$ cm^3 s^{-1} [81]
Loss of Ar metastable atoms			
41	$Ar_m{}^* + e^- \rightarrow Ar^+ + 2\ e^-$	Elec. impact ionization	Electron MC model
42	$Ar_m{}^* + e^- \rightarrow Ar^* + e^-$	Elec. impact excitation	Electron MC model
58	$Ar_m{}^* + e^- \rightarrow Ar_r{}^* + e^-$	Electron quenching	Ar metast. model; $k=2\times10^{-7}$ cm^3 s^{-1} [82]
59	$Ar_m{}^* + Ar_m{}^* \rightarrow Ar^0 + Ar^+ + e^-$	Metast–metast.collision	Ar metast. model; $k=6.4\times10^{-10}$ cm^3 s^{-1} [83,84]
60	$Ar_m{}^* + Cu^0 \rightarrow Ar^0 + Cu^+ + e^-$	Penning ionization of Cu	Ar metast. model; $k=2.6\times10^{-10}$ cm^3 s^{-1} [85,86]
61	$Ar_m{}^* + Ar^0 \rightarrow Ar^0 + Ar^0$	Two-body collision	Ar metast. model; $k=2.3\times10^{-15}$ cm^3 s^{-1} [87]
62	$Ar_m{}^* + 2\ Ar^0 \rightarrow Ar_2{}^* + Ar^0$	Three-body collision	Ar metast. model; $k=1.4\times10^{-32}$ cm^6 s^{-1} [87]
54	$Ar_m{}^* + H_2 \rightarrow Ar + H + H$	Quench. + dissoc. of H_2	Ar metast. model; $k=7\times10^{-11}$ cm^3 s^{-1} [32,73–75]
63	$Ar_m{}^* + H \rightarrow Ar + H^*$	Excitation of H	Ar metast. model $k=4\times10^{-11}$ cm^3 s^{-1} [32]

metastable atoms, because of the possible important role of the metastables in excitation-dissociation of the H_2 molecules (see above). The metastable model used for this purpose has been developed in Bogaerts and Gijbels [76], except that two extra processes are added to the model.

The behavior of the Ar metastable atoms is also described with a balance equation with different production and loss terms, and a transport equation determined by diffusion:

$$\frac{\partial n_{Ar_m*}}{\partial t} + \overline{\nabla} \cdot \overline{j_{Ar_m*}} = R_{prod,\ Ar_m*} - R_{loss,\ Ar_m*}$$
$$\overline{j_{Ar_m*}} = -\ D_{Ar_m*}\overline{\nabla} n_{Ar_m*}$$

The diffusion coefficient (D) was assumed to be 54 cm^2 s^{-1} at 1 torr, like in a pure Ar discharge [76]. The production and loss processes taken into account in the model, as well as the rate coefficients and the corresponding references [81–87], are summarized in Table 3.

The first three production processes, i.e. electron, Ar ion and fast Ar atom impact excitation to the metastable level, are treated in the MC models (see above), and the calculated rates are used as input in the Ar metastable model. A fourth production processes, i.e. Ar ion–electron radiative recombination, is taken into account in the model, although it is actually negligible at the conditions under study [76], due to the small rate coefficient.

The rates of the first two loss processes, i.e. electron impact ionization and total excitation from the metastable level, were also calculated in the electron MC model above, and subsequently used as input in the Ar metastable model. The other loss processes are treated in the metastable model itself, based on the reaction rate coefficients and the densities of the reacting species. Electron quenching (no. 58) means transfer to the nearby 4s resonant levels. Because of the small energy difference between the 4s metastable and resonant levels (see e.g. Bogaerts et al. [77]), this reaction can be carried out by low-energy electrons, and the rate is, therefore, calculated based on the rate coefficient and the Ar metastable and electron density. Collisions between two atoms in metastable levels (no. 59) result in ionization of one of the atoms, whereas the other is de-excited to the ground state. Hence, this process yields the simultaneous loss of two metastable atoms. Although sputtered Cu atoms are not explicitly considered in the present model, Penning ionization of the Cu atoms (no. 60) is taken into account in the Ar metastable model, but a constant value of 5×10^{12} cm^{-3}, which is based on previous model

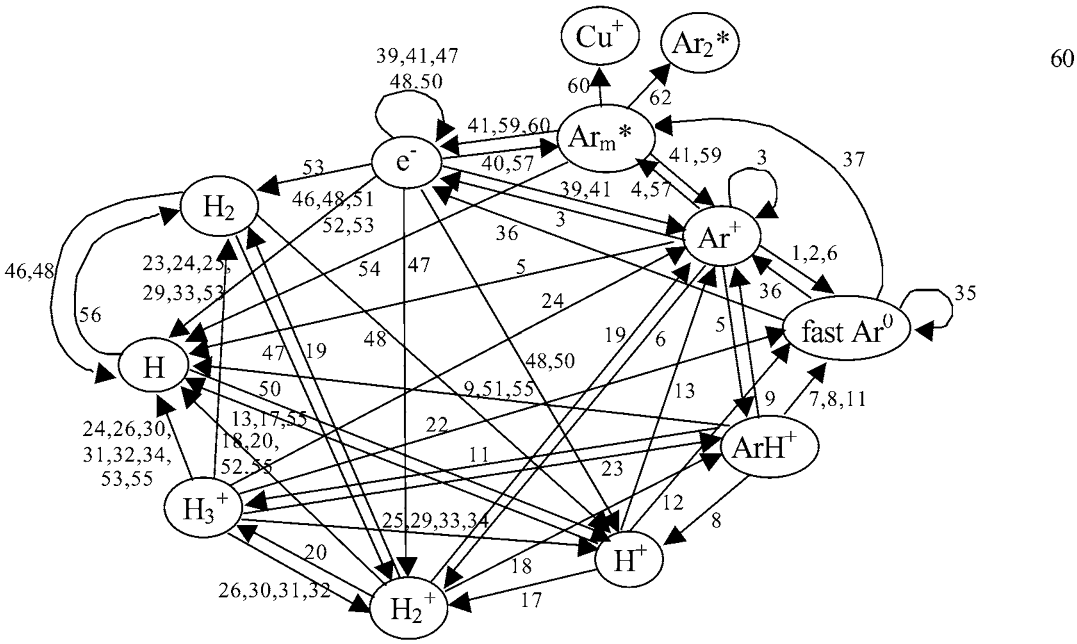

Fig. 8. Diagram illustrating the interactions between the various plasma species, by the reactions taken into account in the model. The numbers in this diagram correspond to the numbers in the text and in Tables 1–3. It should be mentioned that not all interactions (e.g. from H_2 molecules or Ar atoms) are illustrated, in order not to further complicate this figure.

investigations at similar discharge conditions [88], is assumed for the Cu atom density. This is a reasonable approximation, because it has been demonstrated [88] that the contribution of Penning ionization of Cu atoms to the loss of Ar metastable atoms is only a few percent. Two-body and three-body collisions with Ar ground state atoms (nos. 61 and 62) play also only a minor role in the loss of Ar metastable atoms at the conditions under study, but because the rate coefficients are readily available in the literature, and both processes do not significantly increase the computation time, they were also included in the model.

Beside the processes mentioned above, two additional loss processes, related to the hydrogen species, are included in the model. Quenching of Ar metastable atoms by H_2 molecules, resulting in excitation and subsequent dissociation of the H_2 molecules (no. 54) was already discussed above, as being a possibly important candidate to determine the H and H_2 densities in the plasma. Because of the relatively high rate coefficient, in combination with the rather high H_2 density in the plasma, this process might also play a dominant role in determining the Ar metastable density. The last loss process (no. 63) is excitation of H atoms by Ar metastable atoms, leading to de-excitation of the metastable level [22]. The rate coefficient for this process is found in the literature [32] to be 4×10^{-11} cm^3 s^{-1}, for both 4s metastable levels; hence, this value is adopted for the (collective) Ar metastable atoms.

Finally, there is another loss mechanism for the Ar metastable atoms, given by diffusion toward the walls, and subsequent de-excitation at the walls. The boundary condition for this model is again defined based on the method described by Chantry [80] (see above, Section 2.4). More details about this Ar metastable model can also be found in Bogaerts and Gijbels [76].

2.6. Interaction between the different models

It is clear from the above reaction processes that the different plasma species interact with each

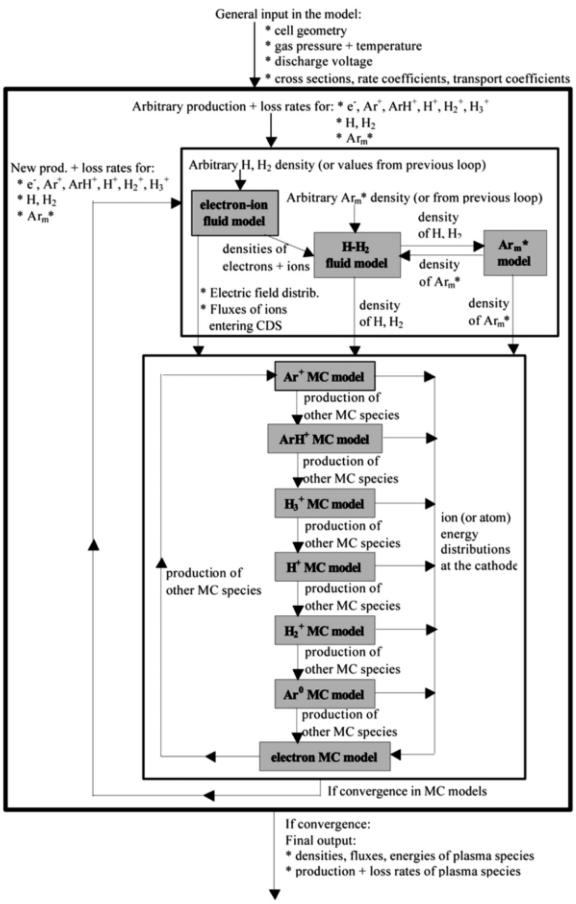

Fig. 9. Flowchart of the entire modeling network, illustrating the coupling between the various models.

other, and that the models used to describe the behavior of these species, should be coupled to each other. Fig. 8 illustrates the interactions between the different plasma species, by the various chemical reactions considered in the models. The numbers correspond to the numbers of the reactions given in Sections 2.1 and 2.2, and in Tables 1–3. This figure is not intended to explain in detail all interactions, but it is only intended to demonstrate that there is a complex interplay between the different species, and hence, that the coupling between the corresponding models is also a quite complicated matter.

Fig. 9 presents a flowchart of the complete modeling network, indicating the different models and the coupling between them (e.g. the output of one model is used as input in the next model). The general input for the modeling network is the cell geometry, the gas pressure and temperature and the voltage, as well as transport coefficients and the cross-sections and rate coefficients of the various processes taken into account in the model. The cell geometry considered in the model corresponds to the standard cell of the VG9000 glow discharge mass spectrometer (see Bogaerts et al. [89] for a schematic picture). It has a cylindrically symmetrical geometry, permitting the calculations to be performed in two dimensions: axial and radial direction. The MC simulations are, however, carried out in three dimensions.

The simulations start with a run of the electron-ion fluid model, using arbitrary production and loss rates for the different species, and arbitrary values for the H atom and H_2 molecule densities (i.e. the H atom density is considered to be zero; the H_2 density is assumed to be 1% of the Ar atom density, which is calculated from the gas pressure and temperature, based on the ideal gas law). This model gives us a first approximation of the electric field distribution in the plasma, the fluxes and density profiles of the various ions and the electrons.

The density profiles of the various ions and the electrons are used as input in the H–H_2 fluid model, which uses, for the first iteration, also arbitrary production and loss rates for the reactions treated in the MC models, and a constant Ar metastable atom density. The results of this H–H_2 fluid model are, among others, the densities of the H atoms and H_2 molecules.

Using the latter density profiles, as well as arbitrary rates for electron, Ar ion and fast Ar atom impact excitation to the metastable levels, and for electron impact excitation and ionization from the metastable levels, a run of the Ar metastable model is carried out, yielding, among others, the Ar metastable atom density.

The latter is inserted in the H–H_2 model, which gives updated results for the H and H_2 density profiles. A second iteration between the Ar metastable model and the H–H_2 fluid model is not necessary here, because the results of both models would not change anymore. Also the coupling back of the $H–H_2$ fluid model to the electron-ion fluid model is not carried out because: (i) the new H and H_2 densities do not affect the calculation results of the electron-ion fluid model to a great extent; and (ii) a new (and unnecessary) run of the electron-ion fluid model increases the overall computation effort of the modeling network.

The electric field distribution, as well as the fluxes of the various ions entering the CDS from the NG, both calculated in the electron-ion fluid model, are used as input in the MC models. Moreover, also the density profiles of the H atoms and H_2 molecules, and of the Ar metastable atoms, calculated with the $H–H_2$ fluid model and with the Ar metastable model, respectively, are inserted in the MC models.

First, the Ar^+ ion MC model is run, using the output from the electron-ion and the $H–H_2$ fluid models, but no input yet from the other MC models (i.e. production rates of Ar^+ ions by other ions or by electrons). The output from this model includes, among others, the Ar^+ ion flux energy distribution at the cathode (required for the electron MC model; see below), and the production of other plasma species (i.e. fast Ar atoms, electrons, Ar metastable atoms, ArH^+ and H_2^+ ions and H atoms). In some cases, where thermal species are created, we just define the production rates of these species as a function of position in the plasma. In most cases, however, where there is energy transfer to the created species, the overall production rate of these species does not give sufficient information, and therefore, the position (z, x, y), energy and direction (axial and azimuthal) of the created species should be written in an array, to be used as input in the other MC models.

Second, the ArH^+ ion MC model is run, using the output from both fluid models and from the Ar^+ ion MC model (i.e. production by H-atom transfer; no. 5). Some of the results, needed as input for the other models, comprise the ArH^+ flux energy distribution at the cathode and the production of other plasma species (i.e. fast Ar atoms, Ar^+, H^+ and H_3^+ ions, and H atoms), again either as the overall production rate, or as the individual coordinates, energy and direction of the created species.

Third, the H_3^+ ions are followed with their MC model, using again the output from both fluid models (i.e. electric field distribution, H_3^+ ion flux entering the CDS from the NG, and H and H_2 density profiles), as well as from the ArH^+ MC model (i.e. production by proton-transfer; no. 11). This model yields again the ion flux energy distribution at the cathode, and the production of other plasma species (i.e. fast Ar atoms, H atoms and H_2 molecules, and Ar^+, ArH^+, H^+ and H_2^+ ions). This model is run before the H^+ and H_2^+ ion MC models, because a lot of different reactions are taken into account, yielding the formation of H^+ and H_2^+ ions, which can then directly be treated in their MC models (instead of waiting for the next iteration loop; see below).

Fourth, the H^+ ion MC model is simulated, using the same data from the electron-ion and $H–H_2$ fluid models, as well as the output from the ArH^+ and H_3^+ MC models (i.e. production rates of H^+ ions), but no input yet from the electron MC model. The results of this model include the H^+ ion flux energy distribution at the cathode, as well as the production of fast Ar atoms, H atoms, Ar^+ and H_2^+ ions.

Fifth, the H_2^+ MC model is run, with the data from both fluid models and from the Ar^+, H^+ and H_3^+ MC models (i.e. production rates of H_2^+ ions), but no input yet from the electron MC model. The output of this model comprises again the ion flux energy distribution at the cathode, as well as the production of H atoms, H_2 molecules, Ar^+, ArH^+ and H_3^+ ions.

Sixth, the fast Ar atoms are simulated with a MC code, using as input the creation rate of fast Ar atoms from the Ar^+, ArH^+, H^+ and H_3^+ MC models. This model gives as output, among others, the fast Ar atom flux energy distribution at the cathode, and the creation of Ar^+ ions, electrons and Ar metastable atoms.

The number of ions followed in the various ion MC models (at least, the number starting at the CDS-NG interface) should be proportional with the corresponding ion flux entering the CDS from the NG. This proportionality factor should in principle be the same for all five different ion species, because of the input/output between the different ion MC models. This would, however, mean that for some ionic species, which are characterized by low fluxes at the CDS-NG interface (e.g. the H^+ and H_2^+ ions; see below), only a small number of ions is followed in the MC models, resulting in bad statistics of the calculation results. On the other hand, the MC simulation for some other ionic species, which have a high flux at the CDS-NG interface, such as the Ar^+ ions, would require a very long calculation time, because a large number of ions is followed, according to this proportionality factor. To overcome this problem, we have applied different proportionality factors for the different ion MC models, but care has to be taken that this manipulation is again compensated for, when using the output of one MC model as input in another MC model. A similar problem arises also for the fast Ar atoms, which are formed in such large numbers by the reaction processes of the various ions, that very long computation times would be required if the same proportionality factor would be used. Therefore, we follow only a fraction (e.g. 20%) of the fast Ar atoms created by the ions, and at the end of this MC run, we multiply all the calculation results (in this example, by a factor of 5). Care should, however, be taken that this fraction is chosen in a statistically justified way.

Finally, the electron MC model is run, using the electric field distribution from the electron-ion fluid model, and the density profiles of H atoms, H_2 molecules and Ar metastable atoms, calculated in the H–H_2 fluid model and in the Ar metastable model, respectively. Other input in this electron MC model, arising from the various ion and the fast Ar atom MC models, are the flux energy distributions of the five different ionic species and the fast Ar atoms bombarding the cathode, which are needed to calculate the electron flux starting at the cathode (see above; Section 2.2), as well as the electron creation rate in the CDS, from Ar^+ ion and fast Ar atom impact ionization (reactions 3 and 36). The output of the electron MC model, of interest for the other models, includes the creation of Ar^+, H_2^+ and H^+ ions, H atoms and Ar metastable atoms, to be used in the ion MC models, in the electron-ion fluid model, in the H–H_2 fluid model, and in the Ar metastable model, respectively.

After having carried out one complete run of all MC models, this run is repeated, having now available all the data (creation of species) from the various MC models. In this way, a number of consecutive runs of all MC models has to be performed, until convergence is reached, which is defined by the ion and Ar atom fluxes arriving at the cathode. Typically, approximately 10 consecutive runs have to be carried out before convergence is reached.

When convergence is reached within the MC models, the electron-ion fluid model, the H–H_2 fluid model, and the Ar metastable model are calculated again, using now the appropriate production and loss rates, as obtained from the MC models (see Tables 1–3). This yields a new electric field distribution, new ion fluxes entering the CDS from the NG, and new density profiles of the plasma species. These new data are then inserted again in the MC models, and the procedure of consecutively running the MC models is repeated, in the same way as above. The iteration between the fluid and metastable models, on one hand, and the various MC models, on the other hand, has to be repeated until final convergence is reached, which takes typically approximately 5–10 iterations, depending on the initial guesses for the production and loss rates. The whole calculation procedure can, therefore, amount to several days on a professional workstation with an alpha-processor.

3. Results and discussion

3.1. Number densities of the plasma species

Fig. 10 shows the calculated two-dimensional density profiles of the various species present in the plasma i.e.: electrons (a); Ar^+ ions (b); ArH^+ ions (c); H^+ ions (d); H_2^+ ions (e); H_3^+ ions (f); H atoms (g); Ar metastable atoms (h); and fast Ar atoms (i), in the VG9000 glow discharge cell, at the discharge conditions investigated here, i.e. 1000 V, 0.56 torr and approximately 2 mA. The cathode is found at the left end of the figures (at $z=0$ cm). The other borders of the figures are at anode potential. Moreover, the black rectangles between $z=0.05$ and $z=0.15$ cm sym-

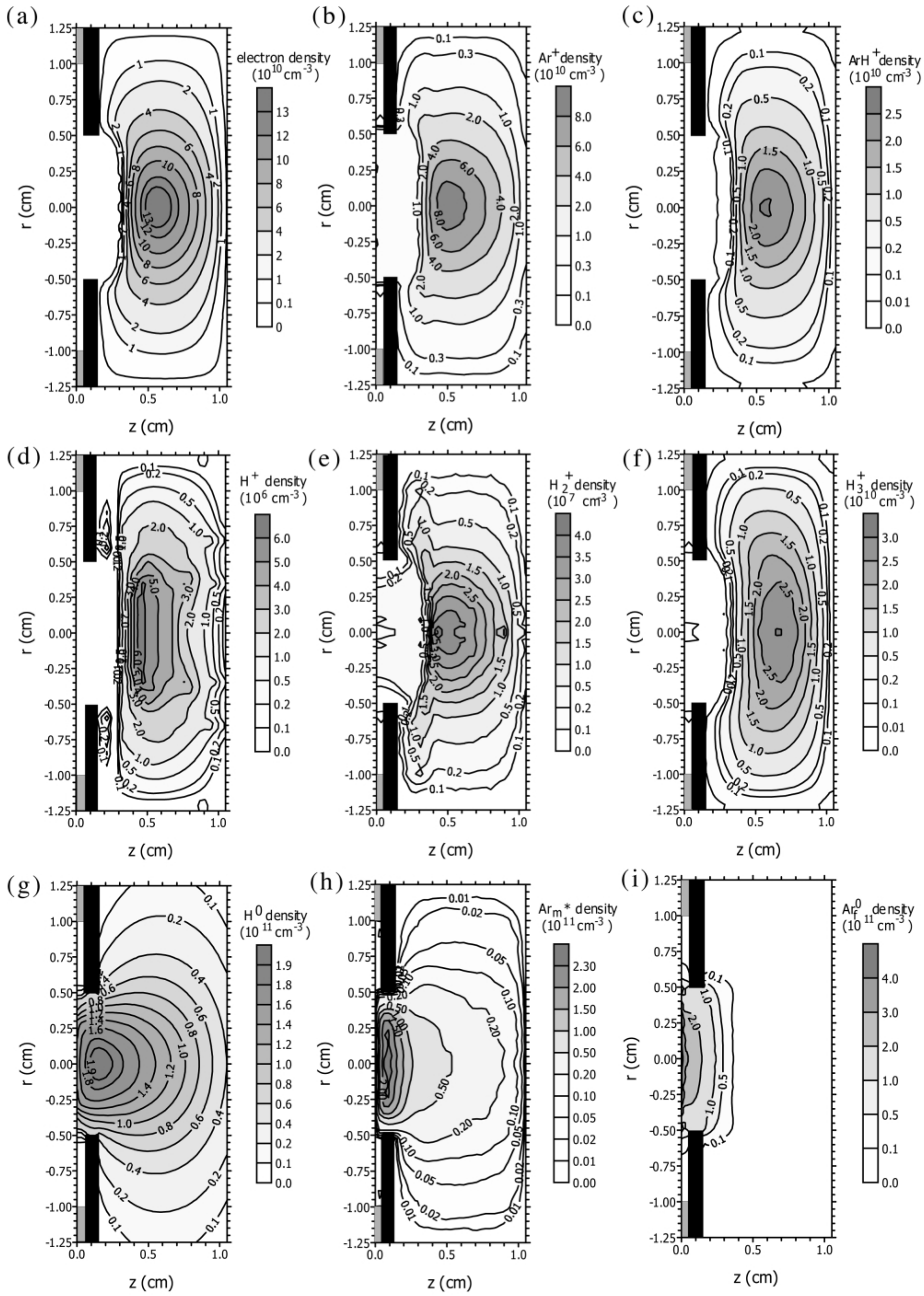

Fig. 10. Calculated two-dimensional density profiles of the different plasma species in the Ar/H_2 discharge, at 1000 V, 0.56 torr and 330 K: (a) electrons; (b) Ar^+ ions; (c) ArH^+ ions; (d) H^+ ions; (e) H_2^+ ions; (f) H_3^+ ions; (g) H^0 atoms; (h) Ar_m^* metastable atoms; (i) fast Ar^0 atoms. The results are presented in the commercial VG9000 glow discharge cell, in which the cathode is found at the left end of the figure, the other borders of the figure, as well as the front-plate (black rectangles between $z=0.05$ and 0.15 cm) are at anode potential, and the gray rectangles between $z=0$ and 0.05 cm represent the insulating ring between cathode and anode.

bolize the so-called 'front-plate' of the cell, which is also at anode potential, whereas the gray rectangles between $z=0$ and $z=0.05$ cm stand for the insulating ring between cathode and anode. The density profiles of Ar gas atoms and H_2 molecules are not shown, because they are found constant throughout the discharge. Indeed, the number density of the background Ar gas at 0.56 torr and 330 K is simply assumed constant and is calculated, based on the ideal gas law, to be equal to 1.65×10^{16} cm^{-3}. The number density of the H_2 molecules was calculated in the H–H_2 fluid model, and was also found to be roughly uniform throughout the discharge, with a value of 1.65×10^{14} cm^{-3}, i.e. exactly 1% of the Ar gas atom density, which was given as input (initial condition) in the model.

The number density profiles of the electrons and the various ionic species (a–f) reach a maximum at approximately 0.5 cm from the cathode, which is halfway the discharge cell, in the NG. The electron density is more or less zero in the CDS (which ranges till approx. 0.3–0.4 cm from the cathode, at the conditions under study), whereas the various ion densities are characterized by low and rather constant (but non-zero) values in this region. The electron density (Fig. 10a) has a maximum of almost 1.4×10^{11} cm^{-3}, whereas the maximum Ar^+ ion density (Fig. 10b) is approximately 9×10^{10} cm^{-3}. These maximum values are reached in the NG. Because the total ion density should be equal to the electron density in the NG, based on the quasi-neutrality condition, this means that the Ar^+ ions are the dominant ionic species in the plasma, at the conditions under study. However, the ArH^+ and H_3^+ ions have also rather high densities, with a maximum of approximately 2.6×10^{10} and 3×10^{10} cm^{-3}, respectively (see Fig. 10c,f). The densities of the H^+ and H_2^+ ions, on the other hand, are found to be negligible at the conditions under study (i.e. with maximum densities in the order of 6×10^6 and 4×10^7 cm^{-3}, respectively; see Fig. 10d,e). These results are, at least qualitatively, consistent with findings in the literature. Indeed, it is reported in Dexter et al. [39] and Simko et al. [40] for pure H_2 discharges that H^+ and H_2^+ ions react rapidly in low-field regions with H_2 molecules to form H_3^+ ions, which do not fragment again, until they move into higher field regions. H_3^+ ions are, therefore, the dominant hydrogen ions in low-field H_2 plasmas [39,40,90,91]. Moreover, in glow discharge mass spectrometry (GDMS) the ArH^+ ion intensities in the mass spectrum are often found of the same magnitude or even higher than the Ar^+ ion intensity, when small amounts of H_2 (or H_2O) are added to the Ar glow discharge [7,92]. Note that the ratios in the calculated ion densities illustrated in Fig. 10 are also reflected back in the ratios of the fluxes of the different ionic species.

The H^0 atom density, as calculated in the H–H_2 fluid model, was found to reach a maximum of nearly 2×10^{11} cm^{-3} at approximately 1 mm from the cathode, and it decreases gradually toward the cell walls (see Fig. 10g). When comparing to the H_2 density of 1.65×10^{14} cm^{-3}, this gives a dissociation degree of H_2 of approximately 2×10^{-4} (or 0.02%). This value is lower than would be expected from the maximum values of the H and H_2 densities, but it is obtained by integration of the densities over the entire discharge cell, and the H atom density drops considerably when moving away from the maximum whereas the H_2 molecules keep their high density throughout the entire discharge. Although the dissociation degree appears to be low, it is still 1–2 orders of magnitude higher than the ionization degree of Ar at the conditions under study (typically 10^{-5}–10^{-6}) [88]. Moreover, in spite of this low dissociation degree, the H atoms have still a quite high density (even higher than the electrons or any of the ionic species); hence they can be considered as one of the major plasma species.

The Ar metastable atoms also reach a maximum density at approximately 1 mm from the cathode, as is illustrated in Fig. 10h. This maximum is slightly higher (i.e. approximately 2.5×10^{11} cm^{-3}) than the H atom density, but the Ar metastable atom density drops much faster to low values in the rest of the plasma.

Finally, the fast Ar atom density is presented in Fig. 10i. Because the fast Ar atoms are created by collisions of fast ions (or other fast Ar atoms), and because fast ions are only present in the CDS, where they are accelerated by the strong electric field, consequently fast Ar atoms are only found in the CDS. Indeed, they are created in this region, and in principle they could travel to the NG, but they will also lose their energy by collisions, and most of them will be thermalized before reaching the NG. This explains why the fast Ar atom density reaches a maximum near the cathode, and is roughly zero in the NG. Even in the CDS, the fast Ar atom density (i.e. $1–4\times10^{11}$ cm^{-3}) is approximately 5 orders of magnitude lower than the background Ar gas atom density of 1.65×10^{16} cm^{-3}. This means that as a whole the Ar atoms can be considered to be thermalized. Nevertheless, this small group of fast Ar atoms plays an important role in the glow discharge plasma, e.g. for fast Ar atom impact ionization [89,93] and excitation [76,88] and for sputtering [88,94].

3.2. Production and loss processes for the different plasma species

In order to understand better the effect of hydrogen on an Ar glow discharge, the various production and loss processes for the different species in the Ar–H_2 discharge are investigated in some more detail. Table 4 presents the relative contributions, integrated over the entire discharge volume, of the most important production and loss processes for the various species. Note that the plasma species also get lost at the walls (e.g. by recombination for electrons and ions, or by de-excitation for the metastables). This is not explicitly counted as a loss mechanism in the balance equations, but it is treated as the boundary condition of the equations. Its relative contribution to the overall loss of the plasma species is, therefore, not included in the table, because it is not so straightforward to estimate. Nevertheless, it is expected to play a non-negligible role. Furthermore, it is worth mentioning that the production and loss mechanisms of the H_2 molecules given in Table 4 are not so important in absolute numbers, because they have nearly no effect in determining the H_2 density. Indeed, the H_2 density calculated in the H–H_2 fluid model is 1.65×10^{14} cm^{-3}, which is exactly 1% of the Ar gas atom density, as was used as input (initial condition) in the model (see Section 3.1).

3.3. Comparison of the Ar/H_2 discharge with a pure Ar discharge

A comparison is also made between a pure Ar discharge and an Ar discharge with 1% H_2. Fig. 11 shows the one-dimensional density profiles of the electrons, the Ar^+ ions and the Ar metastable atoms (at the cell axis, as a function of distance from the cathode), in the Ar+1% H_2 discharge, compared to a pure Ar discharge (solid and dashed lines, respectively). The densities of these species drop considerably with the addition of 1% H_2 (i.e. a factor of 1.4 for the electrons, a factor of 2 for the Ar^+ ions, and a factor of 2.4 for the Ar metastable atoms). A drop in electron and Ar^+ ion densities was also reported in the literature [9–11].

The reasons for this drop become clear when investigating the relative contributions of the various production and loss mechanisms, presented in Table 4. For the electrons, the dominant production is electron impact ionization of Ar, and the production processes related to hydrogen are of minor importance. Although the ionization of Ar might be slightly affected through changes in the electric field, as a result of changes in electron and ion densities, this effect is very small. Hence, the overall production of electrons is not really affected by the addition of H_2. The loss of electrons is, however, attributed to electron-ion recombination with H_3^+ and ArH^+ ions. Because both ions are not present in a pure Ar glow discharge, this means an additional loss in the Ar/H_2 discharge, which explains the lower electron density.

Similarly, for the Ar^+ ions, the production is again mainly due to electron impact excitation of Ar atoms, and the hydrogen-related production mechanisms are of minor importance. As far as the loss of Ar^+ ions is concerned, however, H-atom transfer and (to a less extent) charge transfer with H_2 molecules are together responsible for the entire loss of Ar^+ ions (except of course from recombination at the walls, which is always present as the boundary condition in the model, but which is not explicitly counted in Table 4; see above). These two loss processes are also typical for the Ar/H_2 discharge and are not present in the pure Ar discharge; hence, this explains the drop in

Table 4
Calculated relative contributions of the most important production and loss processes of the various plasma species

Production process	%	Loss process	%
Electrons			
Electron impact ionization of Ar (39)	92.6	Recombination with H_3^+ (53)	61.2
Ar^+ ion impact ionization of Ar (3)	1.4	Recombination with ArH^+ (51)	38.8
Ar^0 atom impact ionization of Ar (36)	5.7		
Electron impact ionization of H_2 (47)	0.3		
Ar^+ ions			
Electron impact ionization of Ar (39)	88.6	H-atom transfer between Ar^+ and H_2 (5)	86.3
Ar^+ ion impact ionization of Ar (3)	1.4	Charge transfer between Ar^+ and H_2 (6)	13.7
Ar^0 atom impact ionization of Ar (36)	5.5		
Charge transfer between H^+ and Ar (13)	2.3		
Charge transfer between H_2^+ and Ar (19)	1.4		
Charge transfer between H_3^+ and Ar (24)	0.3		
CID of ArH^+ by Ar (9)	0.5		
ArH^+ ions			
H-atom transfer between Ar^+ and H_2 (5)	87.7	Proton transfer between ArH^+ and H_2 (11)	94.1
Proton transfer between H_2^+ and Ar (18)	10.5	CID of ArH^+ by Ar (8+9)	3.7
Proton transfer between H_3^+ and Ar (23)	1.8	Electron-ArH^+ recombination (51)	2.2
H^+ ions			
CID of H_3^+ ions by Ar (25)	83.6	Charge transfer between H^+ and Ar (13)	99.6
CID of ArH^+ by Ar (8)	15.9	Charge transfer between H^+ and H_2 (17)	0.4
Electron impact dissoc. ioniz. of H_2 (48)	0.4		
H_2^+ ions			
Charge transfer between Ar^+ and H_2 (6)	91.3	Proton transfer between H_2^+ and Ar (18)	73.6
Electron impact ionization of H_2 (47)	4.6	Charge transfer between H_2^+ and Ar (19)	25.5
CID of H_3^+ ions by Ar (26)	3.9	Proton transfer between H_2^+ and H_2 (20)	0.9
Charge transfer between H^+ and H_2 (17)	0.2		
H_3^+ ions			
Proton transfer between ArH^+ and H_2 (11)	99.8	CID of H_3^+ ions by Ar (25+26)	61.8
Proton transfer between H_2^+ and H_2 (20)	0.2	Electron-H_3^+ recombination (53)	19.9
		Proton transfer between H_3^+ and Ar (23)	14.4
		Charge transfer between H_3^+ and Ar (24)	3.7
H atoms			
Dissoc. of H_2 by Ar_m* quenching (54)	45.6	Recombination at the walls (56)	~100
Reflection of H^+, H_2^+, H_3^+ and ArH^+ at the cathode (55)	24.1		
H-atom transfer between Ar^+ and H_2 (5)	7.9		
Charge transfer between H^+ and Ar (13)	6.4		
Electron impact dissoc. excit. of H_2 (46)	4.6		
Electron-H_3^+ recombination (53)	5.4		
Electron-ArH^+ recombination (51)	2.0		
CID of ArH^+ by Ar (9)	2.1		
H_2 molecules			
CID of H_3^+ ions by Ar (25)	51.6	Dissoc. of H_2 by Ar_m* quenching (54)	52.5
Charge transfer between H_2^+ and Ar (19)	20.5	H-atom transfer between Ar^+ and H_2 (5)	18.1
Proton transfer between H_3^+ and Ar (23)	15.1	Proton transf. between ArH^+ and H_2 (11)	12.6
Electron-H_3^+ recombination (53)	9.4	Charge transfer between Ar^+ and H_2 (6)	9.2

Table 4 *(Continued)*

Production process	%	Loss process	%
Charge transfer between H_3^+ and Ar (24)	3.3	Electron impact dissoc. excit. of H_2 (46)	5.3
		Electron impact ionization of H_2 (47)	2.1
Ar metastable atoms			
Electron impact excitation (40)	36.6	Quenching by H_2 (=dissoc. of H_2) (54)	75.3
Fast Ar^+ ion impact excitation (4)	12.3	Quenching by electrons (58)	15.3
Fast Ar^0 atom impact excitation (37)	51.1	Penning ionization by Cu atoms (60)	5.3
		Electron impact excit. from metast. (42)	3.2
		Metastable–metastable collisions (59)	0.7

The numbers between brackets correspond to the numbers given in Sections 2.1 and 2.2 and in Tables 1–3. *Note*: CID stands for 'collision-induced dissociation'.

Ar^+ ion density. The fact that the drop in Ar^+ ion density is a bit more pronounced than the drop in the electron density is attributed to the fact that in the Ar/H_2 discharge, also other ionic species beside Ar^+ ions are present, and that the total ion density should be equal to the electron density in the NG.

The production of Ar metastable atoms is attributed to electron, fast Ar^+ ion and fast Ar^0 atom impact excitation to the metastable levels, which are again not affected by the addition of H_2. The major loss mechanism of the Ar metastable atoms in the Ar/H_2 discharge is quenching by H_2 molecules, which is again not present in the pure Ar discharge. Hence, this additional loss in the Ar/H_2 discharge explains the drop in the Ar metastable density.

As appears from Fig. 11a,b, the CDS becomes slightly longer in the Ar/H_2 discharge. The length of the CDS can be deduced from the position where the electron density starts to become non-zero, and become more or less equal to the ion density. The reasons for this longer CDS are the somewhat lower Ar^+ ion and electron densities.

Finally, in spite of the considerable differences in the species densities, the calculated electrical current in the Ar/H_2 discharge was only slightly lower than in the pure Ar discharge (i.e. 1.75 vs. 2 mA). Indeed, the somewhat lower calculated electron and Ar^+ ion fluxes in the Ar/H_2 discharge seem to be more or less compensated in the model by the additional fluxes of the hydrogen-related ions.

The changes in densities illustrated for the Ar–H_2 and the pure Ar discharge demonstrate that even small amounts of H_2 have a significant effect on the discharge behavior. Hence, it is not unexpected that the analytical characteristics, such as emission intensities and relative sensitivity factors of different elements, change considerably when traces of H_2 (even below 1%) are present in the discharge, and that for reproducible analytical results, the gas conditions (i.e. gas composition, impurities) should also be as reproducible as possible.

4. Conclusion

A hybrid Monte Carlo–fluid model is developed for a dc glow discharge in Ar with 1% H_2. The species considered in the model, are the electrons, Ar^+, ArH^+, H^+, H_2^+ and H_3^+ ions, the fast Ar^0 atoms, the H atoms and H_2 molecules, as well as the Ar metastable atoms. These species are described with a number of fluid models and Monte Carlo models. The background Ar gas atoms are not explicitly treated in the model, but they are assumed to have a uniform number density of 1.65×10^{16} cm^{-3} at the conditions under study (based on the ideal gas law). More than 60 reactions, representing the interactions between the various plasma species, are taken into account, resulting in a strong coupling of the different models.

The model is applied to a dc glow discharge used for mass spectrometry, operating at 1000 V, 0.56 torr and 2 mA. It calculates the densities and fluxes of the various plasma species, as well as the relative contributions of the production and loss mechanisms for the various species. It appears

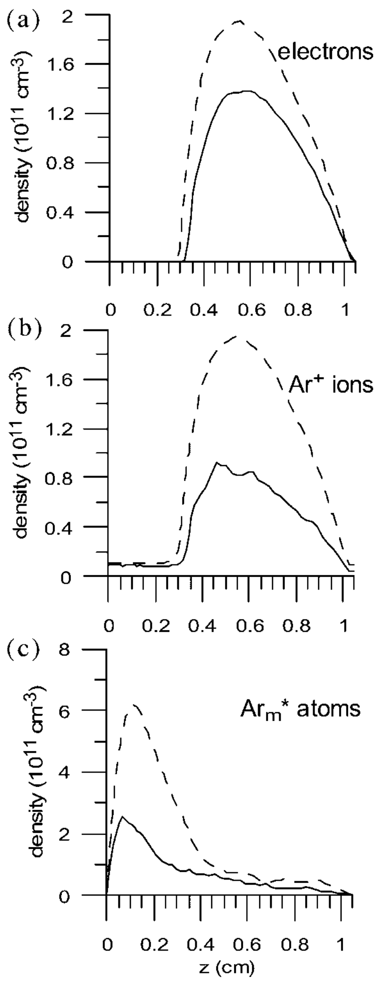

Fig. 11. Calculated one-dimensional density profiles of the electrons (a); Ar^+ ions (b); and Ar_m* metastable atoms (c) in the Ar discharge with 1% H_2 added (solid lines), in comparison to a pure Ar discharge (dashed lines), at the same conditions as in Fig. 10.

that the electrons and the Ar^+ ions have still the highest charged particle density in the plasma (order of 10^{11} cm^{-3}), but the densities of the ArH^+ and H_3^+ ions are less than an order of magnitude lower (a few times 10^{10} cm^{-3}) than the Ar^+ ion density. The H^+ and H_2^+ ions, on the other hand, have much lower densities (order of 10^6–10^7 cm^{-3}), and can therefore be considered negligible at the conditions under study. In spite of a large number of production and loss processes taken into account for the H_2 molecules, the final calculated density of the H_2 molecules is the same as the initial density used as input in the model, i.e. 1% of the Ar gas atom density, or 1.65×10^{14} cm^{-3}. This means that the production and loss processes are not important enough to affect the H_2 density. The H atom density was calculated to be at maximum approximately 2×10^{11} cm^{-3}, which corresponds to a dissociation degree (integrated over the entire discharge region) of approximately 0.02%. This appears to be low, but it is still 1–2 orders of magnitude higher than the typical ionization degree of Ar, at the conditions under study. Finally, the Ar metastable atom density was also in the order of 2×10^{11} cm^{-3}, at the maximum of its profile (i.e. near the cathode), but it drops quite rapidly to low values in the rest of the plasma.

A comparison is also made between the Ar/H_2 discharge and a pure Ar discharge. Both the electron, Ar^+ ion and Ar metastable atom densities drop considerably with the addition of 1% H_2 to the Ar gas. The reason can be found in the production and loss processes of these species. Indeed, the production of these species is attributed to processes such as electron, fast Ar^+ ion and fast Ar^0 atom impact ionization or excitation, respectively, whereas the production processes related to H_2 are of minor importance. Hence, the production of these species is nearly not affected by the addition of H_2. The loss of these species, on the other hand, is mainly due to hydrogen-related processes, e.g. electron-ion recombination with H_3^+ and ArH^+ ions for the electrons, H-atom transfer and charge transfer with H_2 molecules for the Ar^+ ions, and quenching due to H_2 molecules for the Ar metastable atoms. Since these processes are typical for the Ar/H_2 discharge and are not present in a pure Ar discharge, this means an additional loss in the Ar/H_2 discharge, which explains the lower densities of the electrons, Ar^+ ions and Ar metastable atoms.

Also for the other plasma species, the role of the different production and loss processes was investigated. The ArH^+ ions are mainly created by H-atom transfer between Ar^+ ions and H_2 molecules, whereas the loss is mostly due to proton transfer of ArH^+ ions with H_2 molecules. The latter process is also the dominant production mechanism of the H_3^+ ions. These two processes are very efficient, which explains the high densities of ArH^+ and H_3^+ ions. Several processes are responsible for the loss of H_3^+ ions, of which collision-induced dissociation, proton and charge transfer with Ar atoms, as well as recombination with electrons, are the most important (in relative contributions). However, the absolute numbers of these loss rates are not so impressive, which explains again the rather high H_3^+ ion density. The most important production mechanism of the H^+ ions is collision-induced dissociation of H_3^+ ions by Ar atoms, but because the absolute value of this production rate is not very high, the H^+ ion density is rather low. The major loss mechanism of the H^+ ions is charge transfer with Ar atoms. The H_2^+ ions are predominantly created by charge transfer between Ar^+ ions and H_2 molecules, and they are mainly lost by proton or charge transfer of H_2^+ ions with Ar atoms. Because the production process has a rather low rate coefficient and the loss processes (especially proton transfer) are characterized by a high rate coefficient, this explains the low density of the H_2^+ ions, as calculated in our model. Finally, the major production mechanism of the H atoms is dissociation of H_2 molecules by Ar metastable atoms, which appears to be much more important than dissociative excitation by electrons, as was already suggested in the literature [6]. Dissociation of H_2 by Ar metastable atoms is also the major loss mechanism for the H_2 molecules, whereas collision-induced dissociation of H_3^+ ions by Ar atoms appears to be the main production process. Nevertheless, the different production and loss mechanisms taken into account in our model for the H_2 molecules, have nearly no effect on the final calculated H_2 density, which is equal to the initial H_2 density used as input in our model (i.e. 1% of the Ar gas atom density).

It can be concluded that a large number of different processes can occur in the Ar/H_2 discharge, which is much more complicated than a pure Ar discharge. From the changes in densities illustrated for the $Ar–H_2$ and the pure Ar discharge, it is demonstrated that even small amounts of H_2 have a significant effect on the discharge behavior.

Acknowledgments

A. Bogaerts is indebted to the Flemish Fund for Scientific Research (FWO) for financial support. This research is also sponsored by the Federal Services for Scientific, Technical and Cultural affairs (DWTC/SSTC) of the Prime Minister's Office through IUAP-IV (Conv. P4/10). Finally, we are very thankful to A.V. Phelps, for supplying us with the necessary data, for reading the manuscript and for the many interesting discussions.

References

[1] R.K. Marcus, Glow Discharge Spectroscopies, Plenum Press, New York, 1993.

[2] R. Payling, A. Bengtson, D. Jones, Glow Discharge Optical Emission Spectrometry, Wiley, Chichester, 1996.

[3] A. Bengtson, S. Hänström, The influence of hydrogen on emission intensities in GD-OES—consequences for quantitative depth profile analysis, in: R. Tomellini (Ed.), Proceedings of Fifth International Conference on Progress in Analytical Chemistry in the Steel and Metals Industries, European Communities, Luxembourg, 1999, pp. 47–54.

[4] V.-D. Hodoroaba, V. Hoffmann, E.B.M. Steers, K. Wetzig, Emission spectra of copper and argon in an argon glow discharge containing small quantities of hydrogen, J. Anal. At. Spectrom. 15 (2000) 951–958.

[5] V.-D. Hodoroaba, V. Hoffmann, E.B.M. Steers, K. Wetzig, Investigations of the effect of hydrogen in an argon glow discharge, J. Anal. At. Spectrom. 15 (2001) 1075–1080.

[6] V.-D. Hodoroaba, E.B.M. Steers, V. Hoffmann, K. Wetzig, The effect of small quantities of hydrogen on a glow discharge in neon. Comparison with the argon case, J. Anal. At. Spectrom. 16 (2001) 43–49.

[7] R.W. Smithwick III, D.W. Lynch, J.C. Franklin, Relative ion yields measured with a high-resolution glow discharge mass spectrometer operated with an argon/hydrogen mixture, J. Am. Soc. Mass Spectrom. 4 (1993) 278–285.

[8] M. Saito, The relationship between relative sensitivity factors and ionization potential in dc glow discharge mass spectrometry using Ar/0.2 vol.% H_2 mixture, Anal. Chim. Acta 355 (1997) 129–134.

[9] P.F. Knewstubb, A.W. Tickner, Mass spectrometry of ions in glow discharges: I. Apparatus and its application to the positive column in rare gases, J. Chem. Phys. 36 (1962) 674–683.

[10] R.F.G. Meulenbroeks, A.J. van Beek, A.J.G. van Helvoort, M.C.M. van de Sanden, D.C. Schram, Argon–hydrogen plasma jet investigated by active and passive spectroscopic means, Phys. Rev. E 49 (1994) 4397–4406.

[11] R.S. Mason, P.D. Miller, I.P. Mortimer, Anomalous loss of ionization in argon–hydrogen plasma studied by fast flow glow discharge mass spectrometry, Phys. Rev. E 55 (1997) 7462–7472.

[12] M. Capitelli, M. Dilonardo, Nonequilibrium vibrational populations of diatomic species in electrical discharges: effects on the dissociation rates, Chem. Phys. 24 (1977) 417–427.

[13] F.L. Tabares, D. Tafalla, Sputtering of metallic walls in Ar/H_2 direct current glow discharges at room temperature, J. Vac. Sci. Technol. A 14 (1996) 3087–3091.

[14] C.V. Budtz-Jorgensen, P. Kringhoj, J. Bottiger, The critical role of hydrogen for physical sputtering with $Ar–H_2$ glow discharges, Surf. Coat. Technol. 116 (1999) 938–943.

[15] J.T. Gudmundsson, Ion energy distribution in H_2/Ar plasma in a planar inductive discharge, Plasma Sources Sci. Technol. 8 (1999) 58–64.

[16] A. Manenschijn, G.C.A.M. Janssen, E. van der Drift, S. Radelaar, Measurement of ion impact energy and ion flux at the rf electrode of a parallel plate reactive ion etcher, J. Appl. Phys. 69 (1991) 1253–1262.

[17] S.B. Radovanov, J.K. Olthoff, R.J. Van Brunt, S. Djurovic, Ion kinetic-energy distributions and Balmer-alpha (H_α) excitation in Ar/H_2 radio-frequency discharges, J. Appl. Phys. 78 (1995) 746–757.

[18] M. Kuraica, N. Konjevic, Line shapes of atomic hydrogen in a plane-cathode abnormal glow discharge, Phys. Rev. A 46 (1992) 4429–4432.

[19] M. Kuraica, N. Konjevic, M. Platisa, D. Pantelic, Plasma diagnostics of the Grimm-type glow discharge, Spectrochim. Acta Part B 47 (1992) 1173–1186.

[20] I.R. Videnovic, N. Konjevic, M. Kuraica, Spectroscopic investigations of a cathode fall region of the Grimm-type glow discharge, Spectrochim. Acta Part B 51 (1996) 1707–1731.

[21] B. Müller, Ch. Ottinger, M. Yang, L_α emission from collisional excitation of H atoms by threshold energy Ar^+ ions, Z. Phys. A 320 (1985) 61–69.

[22] M.A.A. Clyne, M.C. Heaven, K.D. Bayes, P.B. Monkhouse, Energy transfer in collisions of excited Ar ($^3P_{0,2}$) metastable atoms with H(^{2}S) atoms. II. Lyman-α emission profile, Chem. Phys. 47 (1980) 179–188.

[23] K.R. Ryan, I.G. Graham, Ionic collision processes in mixtures of hydrogen and rare gases, J. Chem. Phys. 59 (1973) 4260–4271.

[24] P. Tosi, High-resolution measurements of integral cross sections in ion-molecule reactions from low-energy-guided crossed-beam experiments, Chem. Rev. 92 (1992) 1667–1684.

[25] N. Sadeghi, D.W. Setser, Symmetry constraints in energy transfer between state-selected Ar* ($^3P_2$, $^3P_0$) metastable atoms and ground state H atoms.', Chem. Phys. 95 (1985) 305–311.

[26] N.G. Adams, D.K. Bohme, D.B. Dunkin, F.C. Fehsenfeld, Temperature dependence of the rate coefficients for the reactions of Ar^+ with O_2, H_2 and D_2, J. Chem. Phys. 52 (1970) 1951–1955.

[27] A.E. Roche, M.M. Sutton, D.K. Bohme, H.I. Schiff, Determination of proton affinity from the kinetics of proton transfer reactions. I. Relative proton affinities, J. Chem. Phys. 55 (1971) 5480–5484.

[28] V. Aquilanti, A. Galli, A. Giardini-Guidoni, G.G. Volpi, Ion-molecule reactions in hydrogen-rare-gas mixtures, J. Chem. Phys. 43 (1965) 1969–1973.

[29] C.R. Lishawa, J.W. Feldstein, T.N. Stewart, E.E. Muschlitz, Excitation of continuum radiation in collisions of (1) electrons and (2) metastable argon atoms with H_2 and D_2, J. Chem. Phys. 83 (1985) 133–139.

[30] B.L. Peko, R.L. Champion, Y. Wang, Destruction cross sections for low energy collisions of H_3^+ and rare gas atoms, J. Chem. Phys. 104 (1996) 6149–6153.

[31] B.L. Peko, R.L. Champion, Total cross sections for low energy collisions of H_3^+ with molecular hydrogen and rare gases, J. Chem. Phys. 107 (1997) 1156–1162.

[32] I.N. Brovikova, E.G. Galiaskarov, A.M. Islyaikin, V.I. Svetsov, Kinetic characteristics of production and loss of hydrogen atoms in the positive column of a glow discharge in an $Ar–H_2$ mixture, High Temp. 37 (1999) 503–509.

[33] A. Bogaerts, R. Gijbels, Effects of adding hydrogen to an argon glow discharge: overview of relevant processes and some qualitative explanations, J. Anal. At. Spectrom. 15 (2000) 441–449.

[34] K. Hassouni, T.A. Grotjohn, A. Gicquel, Self-consistent microwave field and plasma discharge simulations for a moderate pressure hydrogen discharge reactor, J. Appl. Phys. 86 (1999) 134–151.

[35] B. Gordiets, M. Pinheiro, E. Tatarova, F.M. Dias, C.M. Ferreira, A. Ricard, A travelling wave sustained hydrogen discharge: modelling and experiment, Plasma Sources Sci. Technol. 9 (2000) 295–303.

[36] P.H. de Haan, G.C.A.M. Janssen, H.J. Hopman, E.H.A. Granneman, Injection of a relativistic electron beam into neutral hydrogen gas, Phys. Fluids 25 (1982) 592–603.

[37] C.F. Chan, C.F. Burrell, W.S. Cooper, Model of positive ion sources for neutral beam injection, J. Appl. Phys. 54 (1983) 6119–6137.

[38] O. Kukumasa, Numerical studies on the optimisation of volume-produced H^- ions in the single chamber system, J. Phys. D Appl. Phys. 22 (1989) 1668–1679.

[39] A.C. Dexter, T. Farrell, M.I. Lees, Electronic and ionic processes and ionic bombardment of the cathode in a DC hydrogen glow discharge, J. Phys. D Appl. Phys. 22 (1989) 413–430.

[40] T. Simko, V. Martisovits, J. Bretagne, G. Gousset, Computer simulations of H^+ and H_3^+ transport para-

meters in hydrogen drift tubes, Phys. Rev. E 56 (1997) 5908–5919.

[41] O. Leroy, P. Stratil, J. Perrin, J. Jolly, Ph. Belenguer, Spatiotemporal analysis of the double layer formation in hydrogen radio-frequency discharges, J. Phys. D Appl. Phys. 28 (1995) 500–507.

[42] M. Yan, W.J. Goedheer, A PIC-MC simulation of the effect of frequency on the characteristics of VHF SiH_4/H_2 discharges, Plasma Sources Sci. Technol. 8 (1999) 349–354.

[43] M. Yan, W.J. Goedheer, Particle-in-cell/Monte Carlo simulation of radio-frequency SiH_4/H_2 discharges, IEEE Trans. Plasma Sci. 27 (1999) 1399–1405.

[44] T.G. Beuthe, J.-S. Chang, Chemical kinetic modelling of non-equilibrium Ar–H_2 thermal plasmas, Jpn J. Appl. Phys. 38 (1999) 4576–4580.

[45] A.V. Phelps, The application of scattering cross sections to ion flux models in discharges sheaths, J. Appl. Phys. 76 (1994) 747–753.

[46] A.V. Phelps, Cross sections and swarm coefficients for nitrogen ions and neutrals in N_2 and argon ions and neutrals in Ar for energies from 0.1 eV to 10 keV, J. Phys. Chem. Ref. Data 20 (1991) 557–573.

[47] A.V. Phelps, Collisions of H^+, H_2^+, H_3^+, ArH^+, H^-, H and H_2 with Ar and of Ar^+ and ArH^+ with H_2 for energies from 0.1 eV to 10 keV, J. Phys. Chem. Ref. Data 21 (1992) 883–897.

[48] A.V. Phelps, private communication, and ftp://jila.colorado.edu/collision_data

[49] P.S. Krstic, D.R. Schultz, Consistent definitions for, and relationship among, cross sections for elastic scattering of hydrogen ions, atoms and molecules, Phys. Rev. A 60 (1999) 2118–2130, also: http://www-cfadc.phy.ornl.gov/elastic/elasticAr.html.

[50] R.K. Janev, J.J. Smith, Cross sections for collision processes of hydrogen atoms with electrons, protons and multiply charged ions, Atomic and Plasma-Material Interaction Data for Fusion, 4, IAEA, Vienna, 1993.

[51] A.V. Phelps, Cross sections and swarm coefficients for H^+, H_2^+, H_3^+, H, H_2 and H^- in H_2 for energies from 0.1 eV to 10 keV, J. Phys. Chem. Ref. Data 19 (1990) 653–675.

[52] T. Tabata, T. Shirai, Analytic cross sections for collisions of H^+, H_2^+, H_3^+, H, H_2 and H^- with hydrogen molecules, Atom. Data Nucl. Data Tables 76 (2000) 1–25.

[53] H.F. Winters, H. Coufal, C.T. Rettner, D.S. Bethune, Energy transfer from rare gases to surfaces: Collisions with gold and platinum in the range 1–4000 eV, Phys. Rev. B 41 (1990) 6240–6256.

[54] H. Coufal, H.F. Winters, H.L. Bay, W. Eckstein, Energy transfer from noble-gas ions to surfaces: collisions with carbon, silicon, copper, silver and gold, in the range 100–4000 eV, Phys. Rev. B 44 (1991) 4747–4758.

[55] Z. Donko, Apparent secondary-electron emission coefficient and the voltage-current characteristics of argon glow discharges, Phys. Rev. E, 64 (2001) 026401.

[56] Z.Lj. Petrovic, B.M. Jelenkovic, A.V. Phelps, Excitation by and surface reflection of fast hydrogen atoms in low-pressure hydrogen discharges, Phys. Rev. Lett. 68 (1992) 325–328.

[57] A.V. Phelps, Z.Lj. Petrovic, Cold-cathode discharges and breakdown in argon: surface and gas phase production of secondary electrons, Plasma Sources Sci. Technol. 8 (1999) R21–R44.

[58] J.A. Ray, C.F. Barnett, B. Van Zyl, Absolute measurement of low-energy H^0 fluxes by a secondary emission detector, J. Appl. Phys. 50 (1979) 6516–6519.

[59] H. Winter, F. Aumayr, G. Lakits, Recent advances in understanding particle-induced electron emission from metal surfaces, Nuclear Instr. Methods Phys. Res. B58 (1991) 301–308.

[60] A. Bogaerts, R. Gijbels, The ion and atom induced secondary electron emission yield: numerical study for the effect of clean and dirty cathode surfaces, Plasma Sources Sci. Technol. 11 (2002) 27–36.

[61] H.A. Hyman, Electron-impact ionization cross sections for excited states of the rare gases (Ne, Ar, Kr, Xe), cadmium and mercury, Phys. Rev. A 20 (1979) 855–859.

[62] H.A. Hyman, Electron-impact excitation of metastable argon and krypton, Phys. Rev. A 18 (1978) 441–446.

[63] S.J. Buckman, A.V. Phelps, Vibrational excitation of D_2 by low energy electrons, J. Chem. Phys. 82 (1985) 4999–5011.

[64] H. Tawara, Y. Itikawa, H. Nishimura, M. Yoshino, Cross sections and related data for electron collisions with hydrogen molecules and molecular ions, J. Phys. Chem. Ref. Data 19 (1990) 617–636.

[65] A.G. Engelhardt, A.V. Phelps, Elastic and inelastic collision cross sections in hydrogen and deuterium from transport coefficients, Phys. Rev. 131 (1963) 2115–2128.

[66] A. Bogaerts, R. Gijbels, W.J. Goedheer, Hybrid Monte Carlo–fluid model of a direct current glow discharge, J. Appl. Phys. 78 (1995) 2233–2241.

[67] J.O. Hirschfelder, C.F. Curtiss, R.B. Bird, Molecular Theory of Gases and Liquids, Wiley, New York, 1964.

[68] K.B. McAfee, D. Sipler, D. Edelson, Mobilities and reactions of ions in argon, Phys. Rev. 160 (1967) 130–135.

[69] E.E. Ferguson, Rate constants of thermal energy binary ion-molecule reactions of aeronomic interest, Atom. Data Nucl. Data Tables 12 (1973) 159–178.

[70] J.D.P. Passchier, W.J. Goedheer, Relaxation phenomena after laser-induced photodetachment in electronegative rf discharges, J. Appl. Phys. 73 (1993) 1073–1079.

[71] J.D.P. Passchier, W.J. Goedheer, A two-dimensional fluid model for an argon rf discharge, J. Appl. Phys. 74 (1993) 3744–3751.

[72] D.L. Scharfetter, H.K. Gummel, Large-signal analysis of a silicon read diode oscillator, IEEE Trans. Electron. Devices 16 (1969) 64–77.

[73] L.G. Piper, J.E. Velazco, D.W. Setser, Quenching cross sections for electronic energy transfer reactions between metastable argon atoms and noble gases and small molecules, J. Chem. Phys. 59 (1973) 3323–3340.

[74] M. Bourène, J. Le Calvé, De-excitation cross sections of metastable argon by various atoms and molecules, J. Chem. Phys. 58 (1973) 1452–1458.

[75] J.E. Velazco, J.H. Kolts, D.W. Setser, Rate constants and quenching mechanisms for the metastable states of argon, krypton and xenon, J. Chem. Phys. 69 (1978) 4357–4373.

[76] A. Bogaerts, R. Gijbels, Modeling of metastable argon atoms in a direct-current glow discharge, Phys. Rev. A 52 (1995) 3743–3751.

[77] A. Bogaerts, R. Gijbels, J. Vlcek, Collisional-radiative model for an argon glow discharge, J. Appl. Phys. 84 (1998) 121–136.

[78] J.F. Prince, C.B. Collins, W.W. Robertson, Spectra excited in an argon afterglow, J. Chem. Phys. 40 (1964) 2619–2626.

[79] B.J. Wood, H. Wise, Diffusion and heterogeneous reaction. II. Catalytic activity of solids for hydrogen-atom recombination, J. Chem. Phys. 29 (1958) 1416–1417.

[80] P.J. Chantry, A simple formula for diffusion calculations involving wall reflection and low density, J. Appl. Phys. 62 (1987) 1141–1148.

[81] M.A. Biondi, Studies of the mechanism of electron-ion recombination, Phys. Rev. 129 (1963) 1181–1188.

[82] D.P. Lymberopoulos, D.J. Economou, Fluid simulations of glow discharges: Effect of metastable atoms in argon, J. Appl. Phys. 73 (1993) 3668–3679.

[83] C.M. Ferreira, A. Ricard, Modelling of the low-pressure argon positive column, J. Appl. Phys. 54 (1983) 2261–2271.

[84] C.M. Ferreira, J. Loureiro, A. Ricard, Populations in the metastable and the resonance levels of argon and stepwise ionization effects in a low-pressure argon positive column, J. Appl. Phys. 57 (1985) 82–90.

[85] L.A. Riseberg, W.F. Parks, L.D. Schearer, Penning ionization of Zn and Cd by noble-gas metastable atoms, Phys. Rev. A 8 (1973) 1962–1968.

[86] S. Inaba, T. Goto, S. Hattori, Determination of the Penning excitation cross sections of Mg atoms by He, Ne and Ar metastable atoms, J. Phys. Soc. Jpn 52 (1983) 1164–1167.

[87] K. Tachibana, Excitation of the 1s5, 1s4, 1s3 and 1s2 levels of argon by low-energy electrons, Phys. Rev. A 34 (1986) 1007–1015.

[88] A. Bogaerts, R. Gijbels, Two-dimensional model of a direct current glow discharge: description of the argon metastable atoms, sputtered atoms and ions, Anal. Chem. 68 (1996) 2676–2685.

[89] A. Bogaerts, R. Gijbels, W.J. Goedheer, Two-dimensional model of a direct current glow discharge: description of the electrons, argon ions and fast argon atoms, Anal. Chem. 68 (1996) 2296–2303.

[90] B.M. Penetrante, E.E. Kunhardt, Kinetics of hydrogen thyratron plasmas during the conduction phase, J. Appl. Phys. 59 (1986) 3383–3396.

[91] J. Bretagne, G. Gousset, T. Simko, Ion transport simulation in a low-pressure hydrogen gas at high electric fields by a convective-scheme method, J. Phys. D: Appl. Phys. 27 (1994) 1866–1873.

[92] P.H. Ratliff, W.W. Harrison, The effects of water vapor in glow discharge mass spectrometry, Spectrochim. Acta Part B 49 (1994) 1747–1757.

[93] A. Bogaerts, R. Gijbels, The role of fast argon ions and atoms in the ionization of argon in a direct-current glow discharge: a mathematical simulation, J. Appl. Phys. 78 (1995) 6427–6431.

[94] A. Bogaerts, M. van Straaten, R. Gijbels, Monte Carlo simulation of an analytical glow discharge: motion of electrons, ions and fast neutrals in the cathode dark space, Spectrochim. Acta Part B 50 (1995) 179–196.